DOE/ID-22187

SPATIAL VARIABILITY OF SEDIMENTARY INTERBED PROPERTIES NEAR THE IDAHO NUCLEAR TECHNOLOGY AND ENGINEERING CENTER AT THE IDAHO NATIONAL ENGINEERING AND ENVIRONMENTAL LABORATORY, IDAHO

U.S. GEOLOGICAL SURVEY
WATER-RESOURCES INVESTIGATIONS REPORT 03-4142

Prepared in cooperation with the U.S. DEPARTMENT OF ENERGY

≋USGS
science for a changing world

United States Department of the Interior

U.S. GEOLOGICAL SURVEY
INEEL, MS 1160
P.O. Box 2230
Idaho Falls, Idaho 83403

February 2, 2004

Karl Dreher
Idaho Department of Water Resources
Statehouse
Boise, Idaho 83720

Dear Mr. Dreher:

A copy of the following report is enclosed for your information and use:

"Spatial variability of sedimentary interbed properties near the Idaho Nuclear Technology and Engineering Center at the Idaho National Engineering and Environmental Laboratory, Idaho", U.S. Geological Survey Water-Resources Investigations Report 03-4142, DOE/ID-22187

Copies of this report also are available in PDF format, which can be viewed using Adobe Acrobat Reader at URL: http://pubs.water.usgs.gov/wri034142.

Sincerely,

LeRoy L. Knobel
Deputy Project Chief

Enclosure

SPATIAL VARIABILITY OF SEDIMENTARY INTERBED PROPERTIES NEAR THE IDAHO NUCLEAR TECHNOLOGY AND ENGINEERING CENTER AT THE IDAHO NATIONAL ENGINEERING AND ENVIRONMENTAL LABORATORY, IDAHO

By Kari A. Winfield

U.S. DEPARTMENT OF THE INTERIOR
GALE A. NORTON, Secretary

U.S. GEOLOGICAL SURVEY
CHARLES G. GROAT, Director

CONTENTS

FIGURES

TABLES

CONVERSION FACTORS, ABBREVIATED UNITS, AND VERTICAL DATUM

Multiply	**By**	**To Obtain**
millimeter (mm)	0.03937	inch (in)
centimeter (cm)	0.3937	inch (in)
meter (m)	3.281	foot (ft)
kilometer (km)	0.6214	mile (mi)
square centimeter (cm^2)	0.155	square inch (in^2)
square meter (m^2)	10.76	square foot (ft^2)
square kilometer (km^2)	0.3861	square mile (mi^2)
cubic centimeter (cm^3)	0.06102	cubic inch (in^3)
cubic meter (m^3)	35.31	cubic foot (ft^3)
million cubic meters (10^6 m^3)	810.7	acre-foot (acre-ft)
milliliter (ml)	0.03382	fluid ounce (fl. oz)
gram (g)	0.03527	ounce (oz)
dyne	2.248×10^{-6}	pound-force (lb-f)
centimeters of water (cm-water)	0.01419	pound per square inch (lb/in^2)
gram per cubic centimeter (g/cm^3)	64.4220	pound per cubic foot (lb/ft^3)

Temperature: Degrees Celsius (°C) can be converted to degrees Fahrenheit (°F) by using the formula °F = [1.8 × (°C)] + 32. Degrees Kelvin (K) can be converted to °F by the relation °F = [1.8 × (K - 273)] + 32.

Sea level: In this report "sea level" refers to the National Geodetic Vertical Datum of 1929 (NGVD of 1929, formerly called "Sea-Level Datum of 1929"), which is derived from a general adjustment of the first-order leveling networks of the United States and Canada.

Abbreviated units used in report: cm/s (centimeters per second), rad/s (radians per second), cm^3/s (cubic centimeters per second), ml/hr (milliliter per hour), m^2/g (meters squared per gram).

Acceleration due to gravity is abbreviated g, and is taken to equal 980.7 cm/s^2.

Spatial Variability of Sedimentary Interbed Properties near the Idaho Nuclear Technology and Engineering Center at the Idaho National Engineering and Environmental Laboratory, Idaho

by Kari A. Winfield

Abstract

The subsurface at the Idaho National Engineering and Environmental Laboratory (INEEL) is complex, comprised primarily of thick, fractured basalt flows interbedded with thinner sedimentary intervals. The unsaturated zone can be as thick as 200 m in the southwestern part of the INEEL. The Vadose Zone Research Park (VZRP), located approximately 10 km southwest of the Idaho Nuclear Technology and Engineering Center (INTEC), was established in 2001 to study the subsurface of a relatively undisturbed part of the INEEL. Waste percolation ponds for the INTEC were relocated to the VZRP due to concerns that perched water within the vadose zone under the original infiltration ponds (located immediately south of the INTEC) could contribute to migration of contaminants to the Snake River Plain aquifer.

Knowledge of the spatial distribution of texture and hydraulic properties is important for developing a better understanding of subsurface flow processes within the interbeds, for example, by identifying low permeability layers that could lead to the formation of perched ground-water zones. Because particle-size distributions are easier to measure than hydraulic properties, particle size serves as an analog for determining how the unsaturated hydraulic properties vary both vertically within particular interbeds and laterally within the VZRP. As part of the characterization program for the subsurface at the VZRP, unsaturated and saturated hydraulic properties were measured on 10 core samples from six boreholes. Bulk properties, including particle size, bulk density, particle density, and specific surface area, were determined on material from the same depth intervals as the core samples, with an additional 66 particle-size distributions measured on bulk samples from the same boreholes.

From lithologic logs of the 32 boreholes at the VZRP, three relatively thick interbeds (in places up to 10 m thick) were identified at depths of 35, 45, and 55 m below land surface. The 35-m interbed extends laterally over a distance of at least 900 m from the Big Lost River to the new percolation pond area of the VZRP. Most wells within the VZRP were drilled to depths less than 50 m, making it difficult to infer the lateral extent of the 45-m and 55-m interbeds. The 35-m interbed is uniform in texture both vertically and laterally; the 45-m interbed coarsens upward; and the 55-m interbed contains alternating coarse and fine layers. Seventy-one out of 90 samples were silt loams and 9 out of 90 samples were classified as either sandy loams, loamy sands, or sands. The coarsest samples were located within the 45-m and 55-m interbeds of borehole ICPP-SCI-V-215, located near the southeast corner of the new percolation pond area.

At the tops of some interbeds, baked-zone intervals were identified by their oxidized color (yellowish red to red) compared to the color of the underlying non-baked material (pale yellow to brown). The average geometric mean particle diameter of baked-zone intervals was only slightly coarser, in some cases, than the underlying non-baked sediment. This is likely due to both depositional differences between the top and bottom of the interbeds and the presence of small basalt clasts in the sediment. Core sample hydraulic properties from baked zones within the different interbeds did not show effects from alteration caused during basalt deposition, but differed mainly by texture.

Saturated hydraulic conductivities (K_{sat}) for the 10 core samples ranged from 10^{-7} to 10^{-4} cm/s. Low permeability layers, with K_{sat} values less than 10^{-7} cm/s, within the 35-m and 45-m interbeds may cause perched ground-water zones to form beneath the new percolation pond area, leading to the possible lateral movement of water away from the VZRP.

INTRODUCTION

The Idaho Nuclear Technology and Engineering Center (INTEC), formerly known as the Idaho Chemical Processing Plant (ICPP), is located in the southwestern part of the INEEL covering an area of approximately 0.8 km^2 (figs. 1 and 2). Between 1952 and 1984, organic and chemical wastes produced on site were disposed of in a 183-m-deep injection well, which penetrated the Snake River Plain aquifer. Wastes produced after 1984 were disposed of in two infiltration ponds located directly south of the facility (fig. 2). The first infiltration pond was completed in February 1984 and used through October 1985. The second pond was constructed immediately west of the first pond in October 1985 and used through at least 1995. An annual average of 1.6 million m^3 (430 million gallons) of wastewater was discharged to the deep injection well and the infiltration ponds between 1963 and 1993. An average annual discharge of 2.2 million m^3 (570 million gallons) was delivered to the ponds between 1992 and 1995 (Cecil and others, 1991). The primary chemical components of waste discharged to the ponds from 1992 to 1995 included chloride, fluoride, nitrate, sodium, and sulfate, with more than 90 percent of the radioactivity in pond wastewater attributed to tritium. Water samples collected from wells penetrating the aquifer and perched water zones contained radioisotopes of strontium, cesium, americium, plutonium, and hydrogen (Cecil and others, 1991; Bartholomay and others, 1997; Bartholomay, 1998) as a result of waste disposal practices.

The change from deep injection to infiltration ponding led to the formation of perched water zones beneath the ponds between 1984 and 1988. Lithologic features attributed to controlling these zones included low permeability sedimentary units; dense, unfractured basalt; altered basalt

zones created during emplacement of an overlying flow (referred to as interflow baked zones); and sediment and chemical infilling of fractures where sediments overlie basalt units. Perching likely occurred due to the presence of reduced vertical permeability zones in the subsurface and the high volumes of water discharged to the ponds (Cecil and others, 1991).

The 3-km^2 Vadose Zone Research Park (VZRP) was established in 2001 to study the subsurface hydrology and geochemistry of a relatively undisturbed and uncontaminated area of the INEEL (fig. 2). Concerns that perched water within the vadose zone under the original infiltration ponds at the INTEC could contribute to migration of contaminants to the Snake River Plain aquifer led to the construction of two new percolation ponds approximately 9.5 km southwest of the INTEC facility. The relocation of the percolation ponds prompted the development of the VZRP in order to thoroughly characterize the subsurface, so that as the ponds went online, water moving through the subsurface could be monitored and studied. The VZRP will also serve as an area to conduct intermediate- to large-scale hydrologic experiments. The new ponds are scheduled to receive approximately 4,000 m^3 (1 million gallons) of equipment cooling water each day (Bechtel BWXT Idaho, LLC, 2003).

Previous Investigations

Little work has been done to characterize the unsaturated hydraulic properties of the sedimentary interbeds in the vicinity of the INTEC. Most of the solute transport modeling and measurement of hydraulic properties at the INEEL have been conducted near the Radioactive Waste Management Complex (fig. 1), where potential migration of shallow, buried hazardous waste through the unsaturated zone poses concern for Snake River Plain aquifer quality. Perkins (2003) presents bulk and unsaturated hydraulic property measurements for borehole ICPP-SCI-V-215 (fig. 3), located near the southeast margin of the new percolation pond area for the INTEC facility. Additional information about the subsurface, such as stratigraphic and geophysical data for wells near the INTEC, is pre-
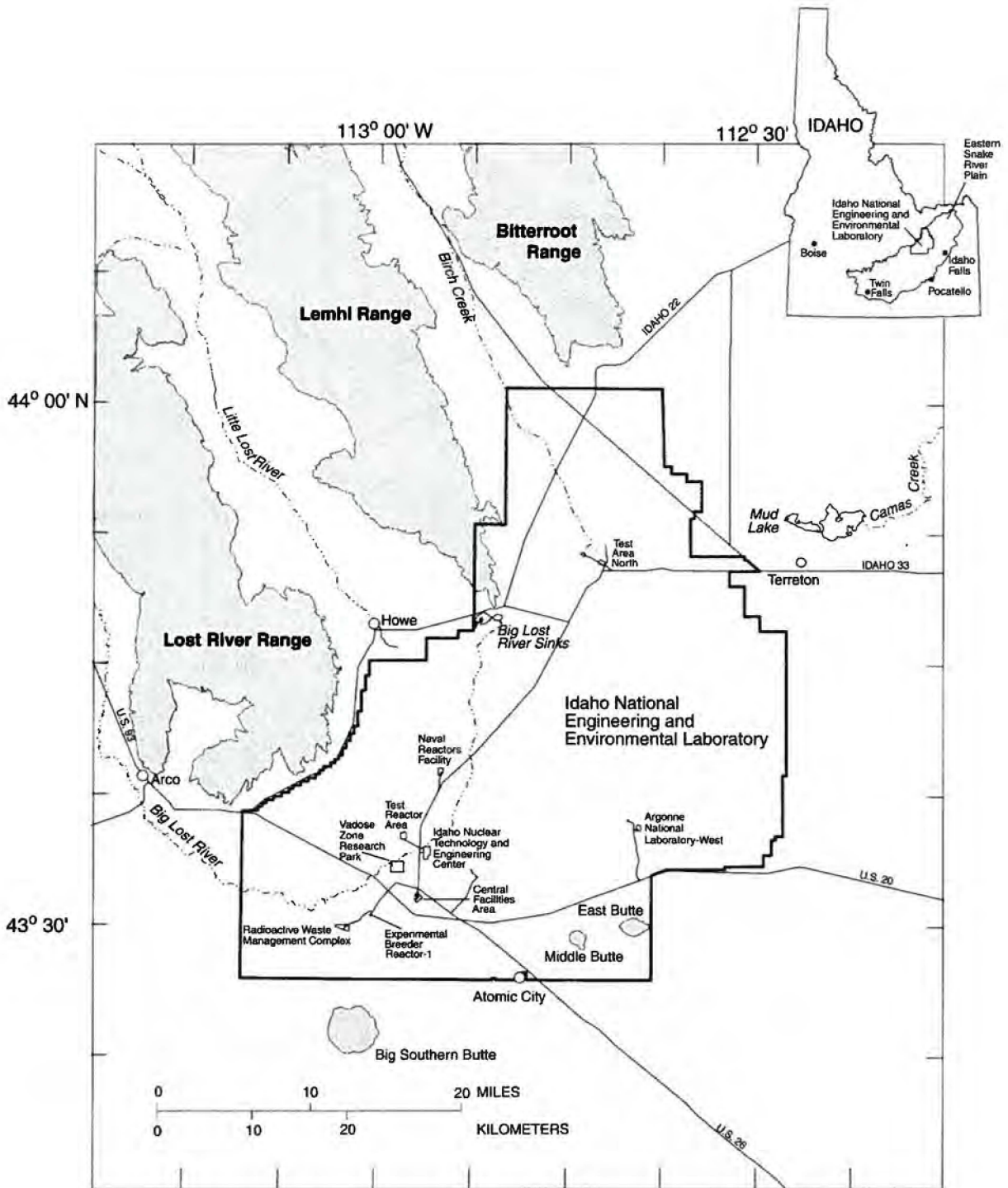
Figure 1. Location of the Idaho National Engineering and Environmental Laboratory, Idaho and selected facilities, including the Idaho Nuclear Technology and Engineering Center.
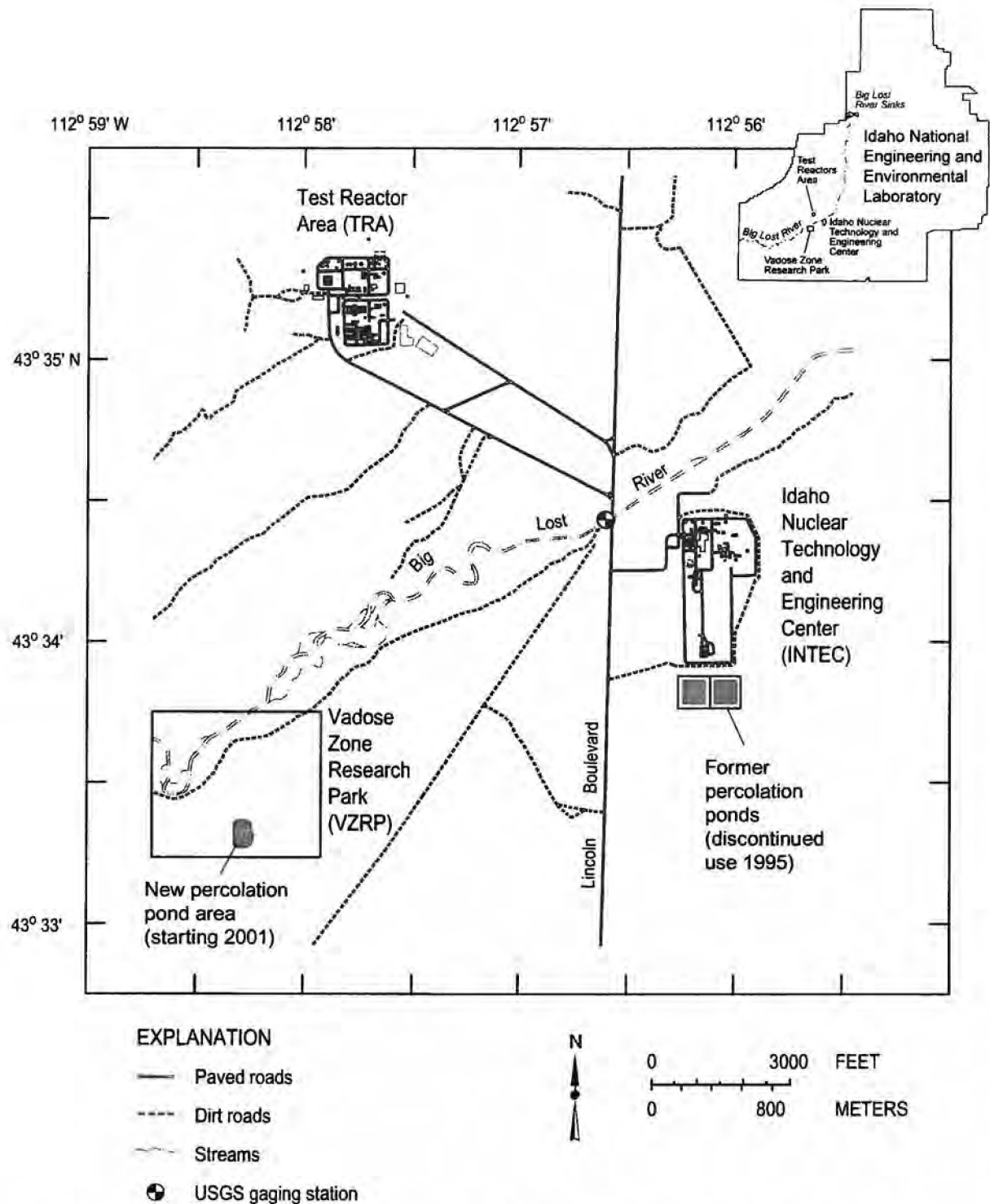
Figure 2. Location of the Vadose Zone Research Park (VZRP) relative to the Idaho Nuclear Technology and Engineering Center (INTEC) and the Big Lost River at the Idaho National Engineering and Environmental Laboratory, Idaho (adapted from the U.S. Geological Survey, 1:24,000 Circular Butte 3 SW quadrangle (1973)). Shown are the former INTEC percolation ponds, located adjacent to the facility, and the new INTEC percolation pond area within the VZRP.
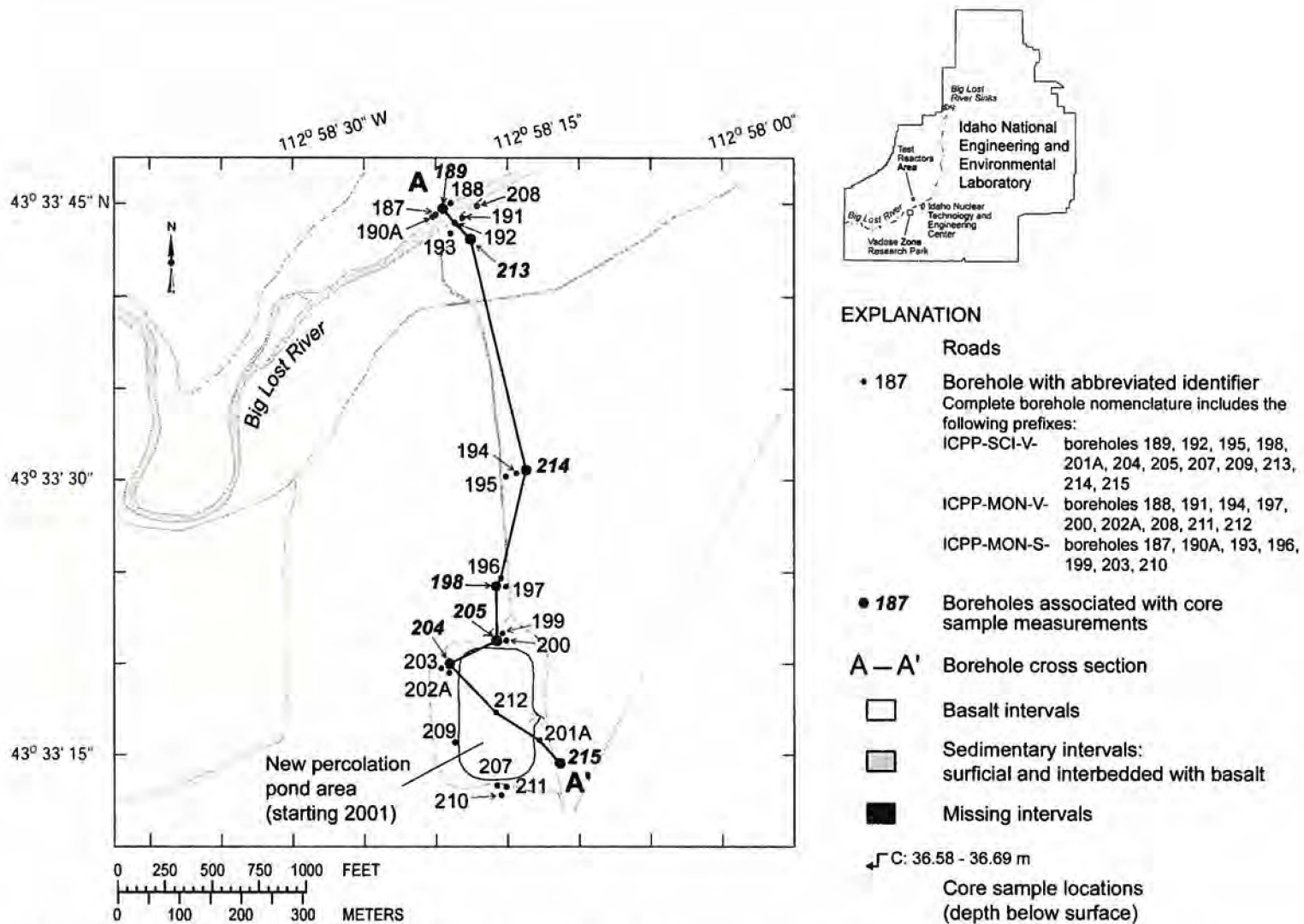
4

Figure 3. Borehole locations within the Vadose Zone Research Park at the Idaho National Engineering and Environmental Laboratory, Idaho (adapted from Bechtel BWXT Idaho, LLC, 2002). Cross section A-A' shows location and thickness of basalt and sedimentary intervals within selected boreholes. Locations of core samples analyzed for unsaturated hydraulic properties are also indicated.

Figure 3. Borehole locations within the Vadose Zone Research Park at the Idaho National Engineering and Environmental Laboratory, Idaho (adapted from Bechtel BWXT Idaho, LLC, 2002). Cross section A-A' shows location and thickness of basalt and sedimentary intervals within selected boreholes. Locations of core samples analyzed for unsaturated hydraulic properties are also indicated—Continued.

sented by Anderson (1991), Anderson and others (1996), and Bechtel BWXT Idaho, LLC (2002).

Purpose and Scope

This report investigates the spatial variability of sedimentary interbed properties measured on core samples from multiple boreholes near the INTEC. Knowledge of the spatial distribution of texture and hydraulic properties is important for developing a better understanding of subsurface flow processes within the interbeds, for example, by identifying low permeability layers that could lead to perching. This type of data is also needed for developing flow and transport models. One goal of the INEEL-Department of Energy contractor, Bechtel BWXT Idaho, LLC, is to correlate the hydraulic and bulk properties of the sedimentary interbeds with their measured geochemical properties in an attempt to delineate possible preferential pathways for subsurface solute transport. The establishment of the VZRP provides a unique opportunity to compare laboratory measurements of unsaturated hydraulic properties with temporal field measurements collected from instruments emplaced at comparable depths to where the core samples were collected. Detailed particle-size information will be useful for applying similar-media scaling (Miller and Miller, 1956; Miller, 1980; Nimmo and others, 2002a) to laboratory-determined hydraulic properties or predicting unsaturated hydraulic properties from more easily measured bulk properties, using transfer functions being developed by scientists at the U.S. Geological Survey (USGS), Menlo Park, CA, or those described in the literature (Arya and Paris, 1981; Schaap, 1999).

Hydraulic and bulk properties were measured on samples from boreholes ICPP-SCI-V-189, -198, -204, -205, -213, and -214 drilled by a subcontractor to the INEEL-DOE contractor Bechtel-BWXT Idaho, LLC and by the USGS in 2000 and 2001. Core sections were collected from three sedimentary interbeds starting at approximately 35, 45, and 55 m below land surface. Because one goal of Bechtel BWXT Idaho, LLC is to compare laboratory and field measurements of hydraulic properties, 1- to 2-foot core sections located at depths comparable to borehole monitoring instru-

ments were selected by Bechtel BWXT Idaho, LLC and sent to the USGS in Menlo Park, CA. The least disturbed intervals were used to re-core smaller samples into the appropriate retainers used with the steady-state centrifuge (SSC) method (Nimmo and others, 1994; Conca and Wright, 1998; Nimmo and others, 2002b) for measurement of unsaturated hydraulic properties. Saturated hydraulic conductivity, saturated water content, hydraulic conductivity as a function of water content ($K(\theta)$) and water retention ($\theta(\psi)$) were measured on 10 re-cored samples. Particle size,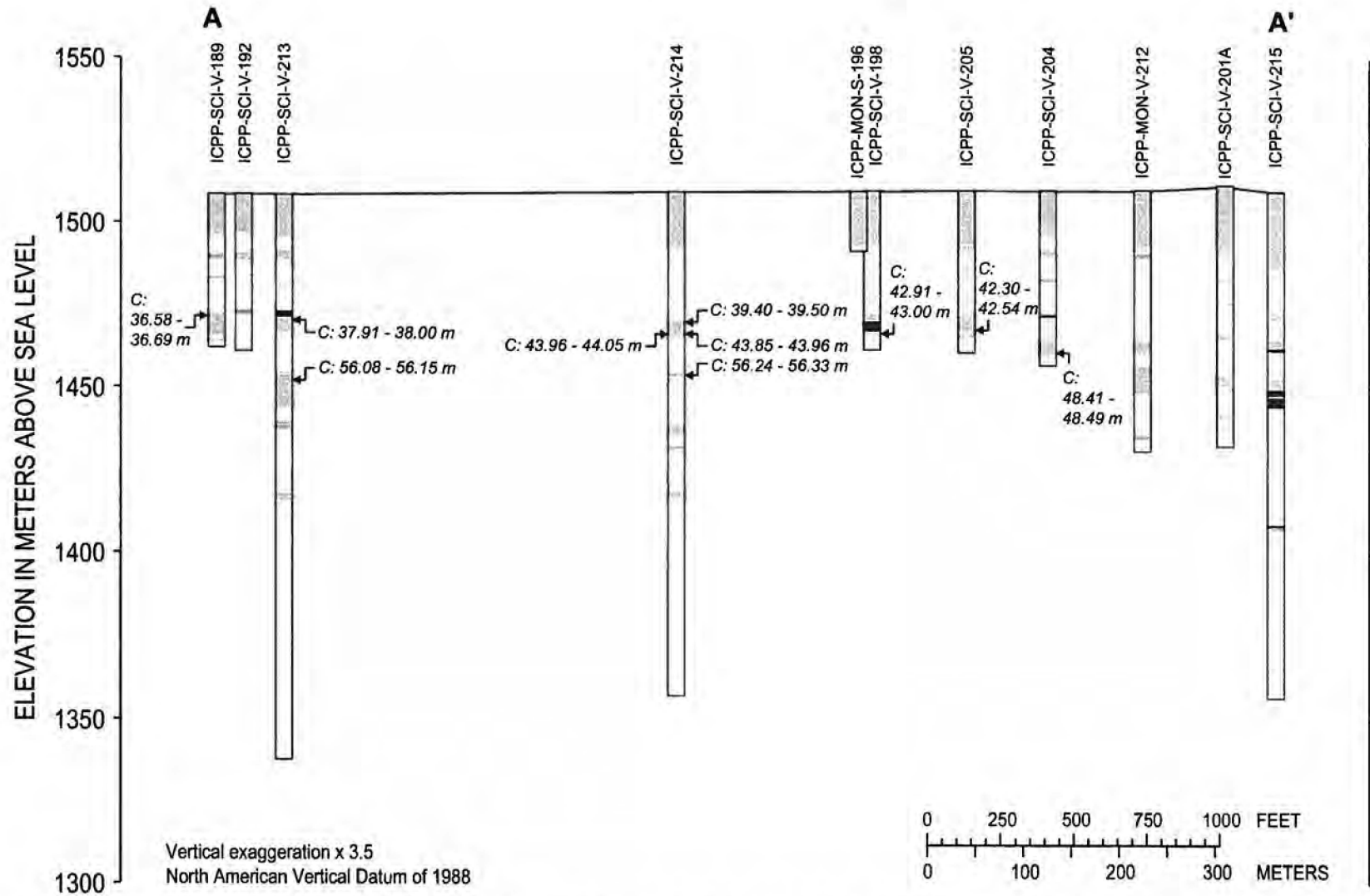 bulk density, particle density, and specific surface area were analyzed on core trimmings saved during sample re-coring. In order to determine the spatial variability of texture within the interbeds, an additional 66 particle-size distributions were measured on bulk samples taken from the longer core sections between the depths of 36 and 57 m, with an average of 13 samples per meter of core received.

Acknowledgments

GEOHYDROLOGIC SETTING

The INEEL occupies about 2,300 km^2 in an active mountain building province on the eastern Snake River Plain, a northern extension of the Basin and Range Province. The eastern Snake River Plain is a northeast trending basin, approximately 320 km long and 80 to 110 km wide, which slopes gently to the southwest and is bordered by northwest trending mountain ranges. Although the area is relatively aseismic, active faults bound these ranges and are involved in their uplift.

The eastern Snake River Plain is underlain by interbedded volcanic and sedimentary units that extend for up to 3000 m below the surface. The sedimentary layers represent quiet intervals between volcanic eruptions and are primarily of eolian, fluvial, and lacustrine origin with large amounts of silt, clay, and sand. Volcanic units, comprised primarily of basalt flows, welded ash flows, and rhyolite, may be vesicular to massive

with either horizontal or vertical fracture patterns. Near the INTEC facility, wells drilled to 200-m depths penetrate a sequence of 23 basalt-flow groups and 15 to 20 sedimentary interbeds (Anderson, 1991). The surficial sediments near the INTEC consist of gravelly alluvium and range from 2- to 20-m thick, being thickest to the northwest (Anderson and others, 1996, figure 7).

The climate of the eastern Snake River Plain is semi-arid with an average annual precipitation of 22 cm. Portions of the Snake River Plain aquifer underlie the INEEL. The depth to the water table ranges from 60 m in the northern part of INEEL to about 200 m toward the south (Barraclough and others, 1981; Liszewski and Mann, 1992). The predominant direction of ground-water flow is from northeast to southwest. Recharge to the aquifer is primarily from irrigation water diversions from streams; precipitation and snowmelt; underflow from streams; and seepage from surface water bodies (Hackett and others, 1986). The Big Lost River is an intermittent stream, which flows from southwest to northeast about 2.5 km north of the new percolation pond area at the INTEC (figs. 2 and 3). The depth to the water table beneath the new percolation ponds is approximately 145 m. A perched water zone has been detected at depths of 35 to 45 m below the new percolation pond area, likely caused by the presence of a low-permeability sedimentary interbed. Waste water exiting the ponds could potentially migrate over large distances within this laterally continuous interbed (Bechtel BWXT Idaho, LLC, 2002).

FIELD AND LABORATORY METHODS

Drilling and Core Collection

Most boreholes were drilled at the VZRP by a subcontractor of Bechtel BWXT Idaho, LLC, with the exception of ICPP-SCI-V-214 and -215, which were drilled by the USGS. Twenty-eight boreholes were completed in the vadose zone (fig. 3) and four boreholes were completed in the Snake River Plain aquifer. The boreholes were drilled between February 2000 and June 2001 using a reverse rotary drilling method. For most holes, air was used as the drilling fluid; water was used in drilling boreholes to lubricate the core barrel.

Boreholes ICPP-SCI-V-189, -192, -195, -198, -204, -205, and -207 were instrumented with advanced tensiometers, suction lysimeters, water content sensors, and soil gas sampling ports at selected depths. Borehole ICPP-SCI-V-214 was instrumented with tensiometers, lysimeters, and gas ports, and ICPP-SCI-V-215 was instrumented with tensiometers and gas ports only. Instrumented boreholes were backfilled with layers of granular bentonite, sand, and silica flour. Core samples were collected in 6.4- and 8.9-cm-diameter Lexan[1] liners at select intervals. Core material analyzed in this study originated from holes ICPP-SCI-V-189, -198, -204, -205, -213, and -214.

The majority of the vadose-zone boreholes were completed to depths ranging from 40 to 50 m below land surface. Seven shallow boreholes (ICPP-MON-S-187, -190A, -193, -196, -199, -203, and -210) do not penetrate beneath the first basalt layer (or greater than about 15 m). Six of the vadose-zone boreholes (ICPP-SCI-V-201A, -209, -213, -214, -215, and ICPP-MON-V-212) were completed to depths greater than 50 m. The four aquifer wells (ICPP-MON-A-164C, -165, -166, and -167; not shown in figure 3) were completed to depths ranging between 160 and 180 m.

Sample Preparation

Ten 0.3- to 0.6-m long core sections from seven boreholes, at depths ranging from 36.5 to 56.4 m (fig. 3), were received by scientists at the USGS, Menlo Park, CA. Subsections of these cores were chosen for bulk and hydraulic property analysis. Most of the sections were disturbed to some degree, as evidenced by the presence of significant fractures along the lengths of the cores, shrinkage of the material away from the liner walls, or looseness of the material within the core liners. The main consequence of this disturbance was difficulty in selecting intact core intervals for use in measuring unsaturated hydraulic properties by the SSC method (Nimmo and others, 1994; Conca and Wright, 1998; Nimmo and others, 2002b). Bulk density values are not likely to be

---

[1]The use of product or company names does not signify their endorsement by the U.S. Geological Survey.

representative of field conditions due to this disturbance.

Because the SSC method requires the use of special sample holders, it was first necessary to select intervals suitable for re-coring into the appropriate centrifuge retainers. The best possible intervals were chosen based on the appearance of the material through the transparent plastic (Lexan[1]) core liners. Intervals with the fewest number of fractures or that appeared most undisturbed and cohesive were selected for re-coring. Shorter, typically 10-cm-long, core sections were created by cutting the liners perpendicular to their lengths using an electric rotary hand tool. To aid in separating the shorter sections from the longer sections after cutting through the liners, a wetting solution (0.3 ml sodium hypochlorite per liter tap water) was applied to the cuts using a squirt bottle. Samples for the centrifuge method were then collected using a re-coring machine designed specifically for minimal disturbance sampling. With the core liner held stationary, a piston pushes material vertically out of the liner while a sharp-edged metal sleeve that houses the centrifuge retainer (located above the core section) shaves the excess material away. Core trimmings were saved for later determination of bulk properties, such as specific surface area, particle density, and particle-size distribution.

Most of the core sections were dry upon their arrival in Menlo Park and, because of their high silt and clay content, very hard. The section from borehole ICPP-SCI-V-214, at 43.75 to 44.36 m depth, appeared to have the highest initial water content. Due to the hardness and dryness of most of the cores, it was necessary to wet the 10-cm-long intervals before re-coring them into the centrifuge sample retainers by submerging them in a dish of the wetting solution.

Hydraulic Properties

Saturated hydraulic conductivity

Prior to measurement of saturated hydraulic conductivity (K_{sat}), each sample in its centrifuge retainer was immersed to its top in a dish of the deaerated wetting solution and wetted to apparent saturation. A wetting solution concentration of 0.3 ml sodium hypochlorite per liter of tap water was used throughout the experiments, including during the determination of unsaturated hydraulic conductivity, in order to inhibit bacterial growth within the soil pores. Saturated water content was calculated on a volume basis by subtracting the oven-dry weight of the core from the wet weight (using the sample weight determined immediately following the K_{sat} experiment) and dividing by the sample volume in the centrifuge retainer.

Two methods were used for K_{sat} measurement (1) the standard falling-head method (Klute and Dirksen, 1986) and (2) a falling-head method adapted for use with a centrifuge (Nimmo and Mello, 1991; Nimmo and others, 2002b). The centrifuge method uses a centrifugal acceleration of approximately 9 g (calculated at the sample midpoint) in addition to gravity to drive flow through the sample. This method is useful when K_{sat} values are expected to be low because samples can reach steady-state conditions more quickly. Saturated hydraulic conductivity (cm/s) using the traditional falling-head method is calculated by:

$$K_{sat} = \left(\frac{aL}{A\Delta t}\right) \ln\left(\frac{H_i}{H_f}\right)$$

where a is the cross-sectional area of the burette (cm^2), A is the cross-sectional area of the sample (cm^2), L is the sample length (cm), H_i and H_f are the initial and final heights of water in the burette (cm), and Δt (s) is the time it takes for the burette level to drop from H_i to H_f. H is defined as the distance between the bottom of the sample and the position of the water meniscus in the burette. K_{sat} (cm/s) by the centrifuge falling-head method is calculated by:

$$K_{sat} = \left(\frac{aL}{A\Delta t}\right) \ln\left(\frac{gH_i + 0.5\omega^2 r_b^2}{gH_f + 0.5\omega^2 r_b^2}\right)$$

where g is the gravitational acceleration (cm/s), ω is the centrifuge speed (rad/s), and r_b is the radius to the bottom of the sample from the center of the centrifuge rotor (cm). Here, H_i and H_f are defined as the initial and final distances between the water level recorded in a burette and the plane in which the sample spins in the centrifuge. Steady-state

9

conditions are achieved when the fluid volume entering the sample equals the effluent volume.

Unsaturated hydraulic properties

The SSC method (Nimmo and others, 1994; Conca and Wright, 1998; Nimmo and others, 2002b) involves using centrifugal force to desaturate samples and define the unsaturated hydraulic conductivity relations, $K(\theta)$ and $K(\psi)$. Darcy's law with the gravitational force term replaced by a centrifugal force term is:

$$q = \frac{Q}{A} = -K_v\left(\frac{d\psi_v}{dr} - \rho_w\omega^2 r\right)$$

where Q is the pump flow rate (cm^3/s), A is the cross-sectional area of the sample (cm^2), K_v is the unsaturated hydraulic conductivity per unit volume (cm^3 s/g), ψ_v is the matric potential per unit volume (dynes/cm^2), ρ_w is the density of water (g/cm^3), ω is the angular velocity of the centrifuge (rad/s), and r is the radius from the center of the centrifuge rotor to the midpoint of the sample (cm). If the centrifugal driving force is applied such that ω is large enough to ensure $d\psi_v/dr \ll \rho_w\omega^2 r$, then any matric potential gradients that develop are insignificant and flow is essentially driven by centrifugal force alone. $K_v(\psi_v)$ is then approximated by $Q/(A\rho_w\omega^2 r)$. Converting to units of pressure head (energy per unit weight), where $K_w \equiv K_v\rho_w g$, this relation becomes:

$$K_w(\psi_w) \approx \frac{Qg}{A\omega^2 r}$$

with K_w expressed in cm/s and ψ_w expressed in cm-water, and where g is the acceleration due to gravity, or 980.7 cm/s^2. (Note that in the remainder of the text, the subscript 'w' will be dropped when referring to matric pressure (ψ)). The unsaturated hydraulic conductivity points that define the $K(\theta)$ relation can then be determined by varying the centrifuge speed and pump flow rate until a constant water content is achieved.

A Beckman[1] model J-6M ultracentrifuge with an Unsaturated Flow Apparatus[1] (UFA) rotor (Conca and Wright, 1998) was used in the SSC method. Infusion pumps were used to deliver flow rates greater than 0.1 ml/hr, while a syringe pump was used to achieve flow rates as low as 0.01 ml/hr. Unsaturated K values ranging from 10^{-10} to 10^{-4} cm/s can be achieved with the SSC method. Two samples of similar texture were run simultaneously, starting from saturation (as determined by the falling-head methods described above) and desaturating in increments determined by varying the pump rate and centrifuge speed. The steady-state criterion was achieved when the sample weight remained constant after repeated spinning of the centrifuge at the same speed and using the same pump flow rate.

After determining the steady-state water content associated with a given unsaturated hydraulic conductivity, the sample was removed from the centrifuge to measure the equilibrium matric pressure (ψ) using a tensiometer or a filter paper. Pairing the average water content (θ) of the sample with the equilibrium pressure yielded a point on the water retention curve ($\theta(\psi)$). ψ is zero at complete saturation and becomes increasingly more negative as the sample desaturates. A tensiometer was used to measure pressures higher than -700 cm-water. At lower (more negative) pressures, air in the tensiometer comes out of solution and expands, causing errors in the ψ measurement. For $\psi < -700$ cm-water, the filter paper method was used. Whatman[1] No. 42 filters, 3.33 cm diameter, were chosen because of the availability of published retention curves for this filter type. The formulas used to determine the matric pressure associated with the gravimetric water content (F) of the filter paper are those of Fawcett and Collis-George (1967) as stated by Greacen and others (1987). For $F < 0.453$:

$$\psi = (-10.2)\exp(12.265 - 17.931F)$$

and for $F > 0.453$:

$$\psi = (-10.2)\exp(5.553 - 3.095F)$$

with ψ expressed in cm-water. A single filter paper was placed in contact with the top of the sample, using a foil-wrapped stopper to make good contact between the sample surface and the filter. The sample was then wrapped in plastic and foil to prevent evaporation. Each sample was

10

allowed to equilibrate with the filter paper for at least 3 days—the midpoint of the equilibration periods indicated in the literature (Fawcett and Collis-George, 1967; Hamblin, 1981; Chandler and Gutierrez, 1986; and Greacen and others; 1987).

Bulk Properties

Bulk density, particle density, and porosity

Bulk density (ρ_b) was determined by dividing the oven-dry weight of the re-cored sample by the total volume. The total volume was calculated from the dimensions of the centrifuge retainer (3.33 cm diameter and 4.9 cm length, on average), with the sample length adjusted for a top recess. Recesses were estimated by taking an average of several measurements over the sample surface with a depth micrometer. The particle density for each sample (ρ_s) was measured by the pycnometer method, after Blake and Hartge (1986), using representative splits of the air-dried core trimmings. Total porosity (Φ) was then calculated from the relation $\Phi = 1 - (\rho_b / \rho_s)$. Initial bulk density and porosity (ρ_{bi} and Φ_i) values represent the state of the samples prior to measurement of unsaturated hydraulic properties in the centrifuge. Final values (ρ_{bf} and Φ_f) were calculated after all centrifuge and water retention measurements were completed.

Particle-size distribution

Prior to particle-size determination, the trimmings saved during re-coring of the SSC samples were air-dried and then physically disaggregated using a rubber-tipped pestle and ceramic mortar. Munsell (1994) colors were assigned to the dry bulk samples after disaggregation. A Gilson[1] 16-part rotary sample divider was used to accurately create small representative subsamples for use in an optical analyzer (Coulter[1] LS 230 Series). The optical analyzer can measure particle sizes ranging from 4×10^{-5} to 2 mm. Because the samples contained no particles greater than 2 mm, sieving was not required prior to splitting. The presence of basalt fragments usually occurred near the interface of the sediment with a basalt layer. Because these were not depositional clasts, basalt frag-

ments were not considered part of a sample's particle-size distribution.

The Coulter[1] LS 230 is a commercially available device that uses a laser to scatter light through a sample suspended in filtered tap water (Gee and Or, 2002). As the sample is circulated through a transparent cell, the diffraction pattern from the laser is measured by a series of detectors. A mathematical algorithm (Fraunhofer diffraction model) is used to convert the diffraction pattern into particle sizes, assuming spherically shaped particles. On a logarithmic scale, the bin size or Δd interval is defined as $\log(d_{upper}) - \log(d_{lower})$, or $\log(d_{upper}/d_{lower})$, where d_{upper} represents the upper bin limit and d_{lower} represents the lower bin limit in terms of particle diameter. By default, the device determines the frequency of particles falling within 116 bins, with an average Δd of 0.041.

Subsamples on the order of 0.5–1 g were created by re-riffling a 1/16th split of the original air-dried core trimmings, with the final amount required for analysis depending on texture. Sonication during loading of the samples and before each analysis was used to further disperse aggregates. The particle-size distribution was measured at least three times on a given subsample, with the average of the best three sequential runs used as the final particle-size distribution of the sample.

The method of moments (Beyer, 1991) was used to calculate the geometric mean particle diameter and standard deviation from each of the measured particle-size distributions. The geometric mean particle diameter (M_g) was calculated by:

$$\log(M_g) = \frac{\sum [f(d_c)\log(d_c)]}{\sum f(d_c)}$$

where d_c is the geometric center of each bin (equal to $\Delta d/2$), and $f(d_c)$ corresponds to the frequency of sizes occurring within each Δd assigned to d_c. The geometric particle-size standard deviation (σ_g) was calculated by:

$$[\log(\sigma_g)]^2 = \frac{\sum \left\{ f(d_c)[\log(d_c) - \log(M_g)]^2 \right\}}{\sum f(d_c)}$$

Specific surface area

Calculations of specific surface area are based on the Brunauer-Emmett-Teller (BET; 1938) theory of nitrogen gas adsorption onto a solid surface. BET theory accounts for multimolecular adsorption of a gas onto a solid, and the subsequent interaction between layers, whereas Langmuir theory assumes a single monolayer and inelastic collision of a gas molecule with the solid surface (Webb and Orr, 1997). Specific surface area is calculated from an adsorption isotherm, defined as the volume of gas adsorbed under various partial pressures onto a solid surface at a constant temperature. The temperature is kept fixed by allowing the sample to come into equilibrium with a bath of liquid nitrogen at 77.35 K at each partial pressure. The BET formula equates the rate of condensation of gas molecules onto an already adsorbed layer to the rate of evaporation from that layer, summed over an infinite number of layers. Rearranging the BET formula into a linear form yields:

$$\frac{P}{V_a(P-P_o)} = \frac{1}{V_m C} + \frac{C-1}{V_m C}\left(\frac{P}{P_o}\right)$$

where V_a is the amount of gas adsorbed at pressure P, V_m is the amount of gas adsorbed when the entire solid surface is covered by a monolayer of the gas molecule, P_o is the saturation pressure of the gas, and C is a constant. Measurements in the BET range of the adsorption isotherm (at very low partial pressures) should follow a linear relationship. Regressing measurements of $P/(V_a(P-P_o))$ against P/P_o yields values of the slope and intercept terms from which C and V_m are calculated. The specific surface area, in m^2/g, is determined by:

$$s = \frac{V_m \sigma N_A}{m V_o}$$

where σ is the mean area occupied per molecule in the monolayer (assumed to be 16.2×10^{-20} m^2 for nitrogen), N_A is Avogadro's number (6.023×10^{23} molecules/mole), V_o is the molecular volume of the gas being adsorbed ($22,414$ cm^3 at standard temperature and pressure for nitrogen), and m is the sample weight (g) (Webb and Orr, 1997).

Specific surface areas were measured for 1–2 g, representative splits of the core trimmings using a Micromeritics[1] TriStar 3000 analyzer. Samples were heated to 105 °C for at least 24 hours prior to analysis in order to evaporate water from the particle surfaces and from within pores, which can lead to errors in the computed values. An additional 2–7 hours of degassing by nitrogen while heating at 105 °C occurred prior to analysis. Five points on the adsorption isotherm were measured to calculate specific surface areas. The sample weight was taken as the weight prior to analysis (after oven-drying and nitrogen degassing).

RESULTS AND DISCUSSION

This study provides information on the hydraulic and bulk properties of sedimentary interbeds at the VZRP located near the INTEC. The measurement of texture and hydraulic properties at multiple borehole locations and depths is important for understanding the spatial distribution of sedimentary interbed properties, developing flow and transport models, and comparing field and laboratory hydraulic measurements. Because measurement of unsaturated hydraulic properties is often time and labor intensive, detailed particle-size data are useful for applying similar-media scaling (Miller and Miller, 1956; Miller, 1980; Nimmo and others, 2002a) to existing hydraulic properties or predicting hydraulic properties using available transfer functions (Arya and Paris, 1981; Schaap, 1999). Particle-size information is also useful for interpreting depositional environments within the interbeds. This report describes the spatial variability of the measured hydraulic and bulk properties of the interbeds beneath the VZRP, as reported in this study and that of Perkins (2003).

Laboratory Measurements

Saturated hydraulic conductivity (K_{sat}), saturated water content (θ_{sat}), and the unsaturated hydraulic relations ($K(\theta)$ and $\theta(\psi)$) were measured on 10 core samples from six boreholes (fig. 3). Particle size, bulk density, particle density, porosity, and specific surface area were measured

on material from the same depths as the SSC core samples. These measurements were made on trimmings saved during sample re-coring. An additional 66 particle-size distributions were measured on bulk samples, with sample intervals ranging in thickness from 6.4 to 25.4 mm, from each of the original 0.3- to 0.6-m-long core sections (on average, 13 measurements per meter of core). Fewer bulk particle-size distributions were measured on core sections containing obviously disturbed material or solid basalt intervals.

Particle density values are reported in table 1 along with the initial bulk density and porosity values (ρ_{bi} and Φ_i), determined prior to measurement of unsaturated hydraulic properties in the centrifuge, and the final values (ρ_{bf} and Φ_f), which were determined after all centrifuge measurements were completed. Compaction as a result of the disturbed state of the samples was observed in most cases as evidenced by an increase in bulk density between the initial and final values.

Values of K_{sat} and θ_{sat} are listed in table 2 for each core sample, including the method used to determine K_{sat}. θ_{sat} values were calculated using the initial bulk density (ρ_{bi}) of the sample (table 1) determined after measurement of K_{sat}. Saturated hydraulic conductivities ranged from 2.07×10^{-7} to 8.31×10^{-4} cm/s, which are typical for samples of silt loam texture. The core sample from ICPP-SCI-V-189 at 36.59 to 36.69 m had a high value of K_{sat}, 8.31×10^{-4} cm/s, compared to the other samples, likely due to macropores within the sample or disturbance caused by handling or drilling.

The measured sets of K, θ, and ψ for each of the 10 core samples are listed in table 3. The first values listed for each sample are θ_{sat} and K_{sat}. The method used to measure ψ at each θ is indicated in a separate column, except for θ_{sat} where a value of -0.1 cm-water was assumed. Water retention curves ($\theta(\psi)$) are shown in figure 4, with measurements indicated by symbols. Curves shown as dotted lines were fit to the measurements using the van Genuchten (1980) function. An average of eight matric pressure values was measured per sample, with measurements sometimes extending beyond the range of θ achieved by the SSC method. Measurements of hydraulic conductivity as a function of water content ($K(\theta)$) are shown in

figure 5. The number of unsaturated K values measured per sample varied depending on texture. Fine-textured samples had fewer points because their lower K_{sat} values meant a smaller range of unsaturated K fell within the measurable range of the SSC method. Because compaction usually occurred after the first unsaturated K measurement and sample recesses were not measured until after the final K measurement, unsaturated water contents were calculated using the final bulk density (ρ_{bf}) of the sample (table 1).

Cumulative particle-size distributions on a percent-finer-than basis are shown in figure 6 for each core sample. Table 4 lists the textural class percentages and textural names for each bulk and core sample based on the U.S. Department of Agriculture's soil classification system (Soil Survey Staff, 1975). Sample textures ranged from silty clay loam, with a maximum clay content of 29 percent, to loam, with a minimum clay content of 7 percent. However, most samples were classified as silt loams. Specific surface areas for each of the 10 SSC samples are given in table 5.

The unsaturated hydraulic properties for two samples taken from vertically adjacent locations in borehole ICPP-SCI-V-214 at depths of 43.85 m and 43.96 m showed conflicting results. Because these samples have closely matched particle-size distributions (fig. 6), their unsaturated hydraulic properties should also agree. The results for the sample at 43.96 to 44.05 m depth are suspect because a gap, likely caused by an error in the re-coring process, was discovered at the bottom of the sample retainer after all K, θ, and ψ measurements were completed. This made it difficult to determine the sample length used in calculating K_{sat}, bulk density, porosity, and θ_{sat}. The effect of this disturbance is also evident in the $K(\theta)$ and $\theta(\psi)$ relations (figs. 4 and 5), where θ is shifted toward lower values, as if the sample texture was coarser than measured.

35-m, 45-m, and 55-m Interbeds

Three relatively thick interbeds were identified from drilling logs (Bechtel BWXT Idaho, LLC, 2002; USGS visual log for ICPP-SCI-V-215, Linda Davis, USGS, personal commun., 2003) of the 32 boreholes located within the VZRP at

13
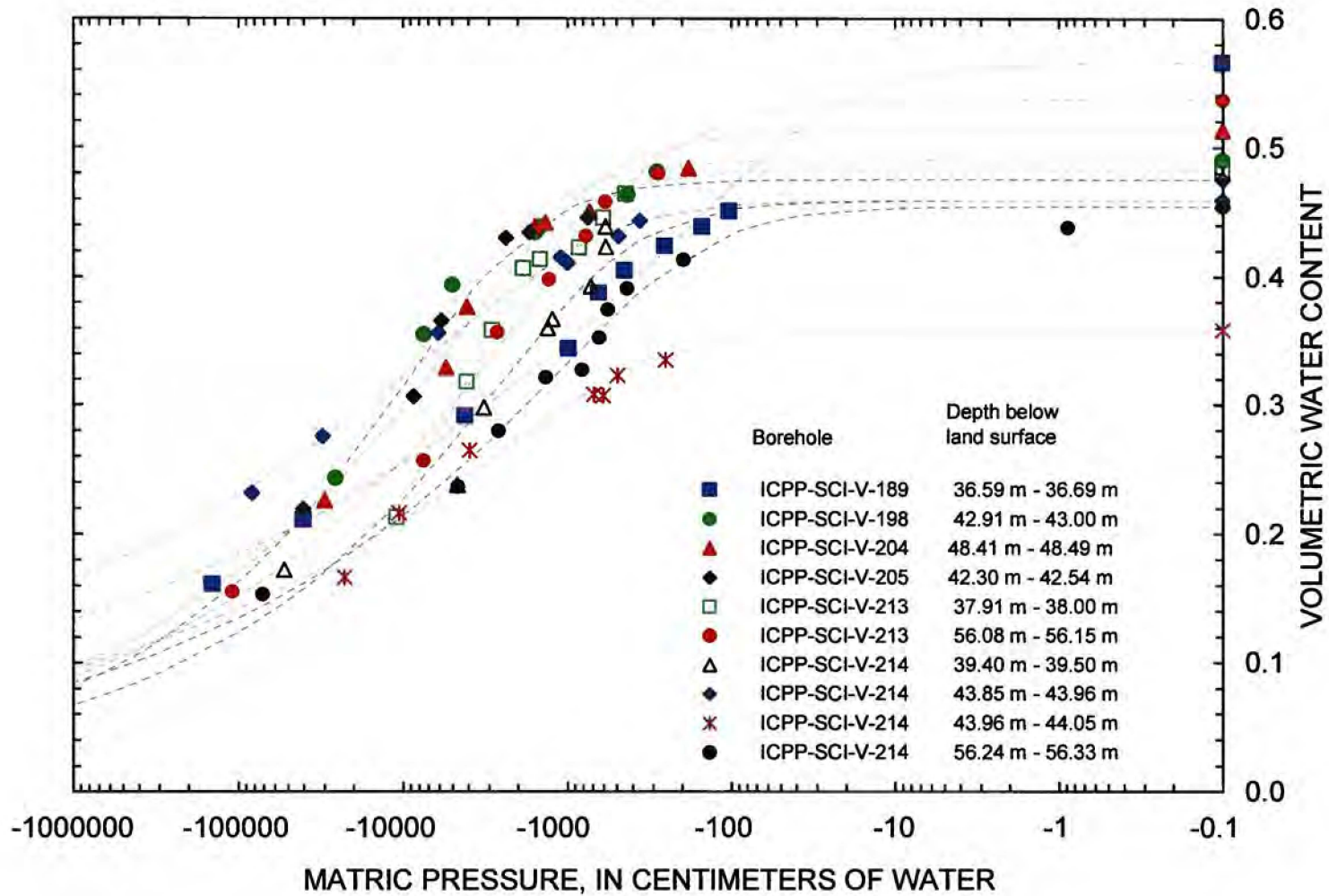
Figure 4. Water content as a function of matric pressure, measured using the steady-state centrifuge method, for 10 sedimentary interbed core samples collected from depths of 36.59 to 56.33 m below land surface within the Vadose Zone Research Park, Idaho National Engineering and Environmental Laboratory, Idaho. Symbols represent measured points and dotted lines represent optimized curves fitted with the van Genuchten (1980) formula.
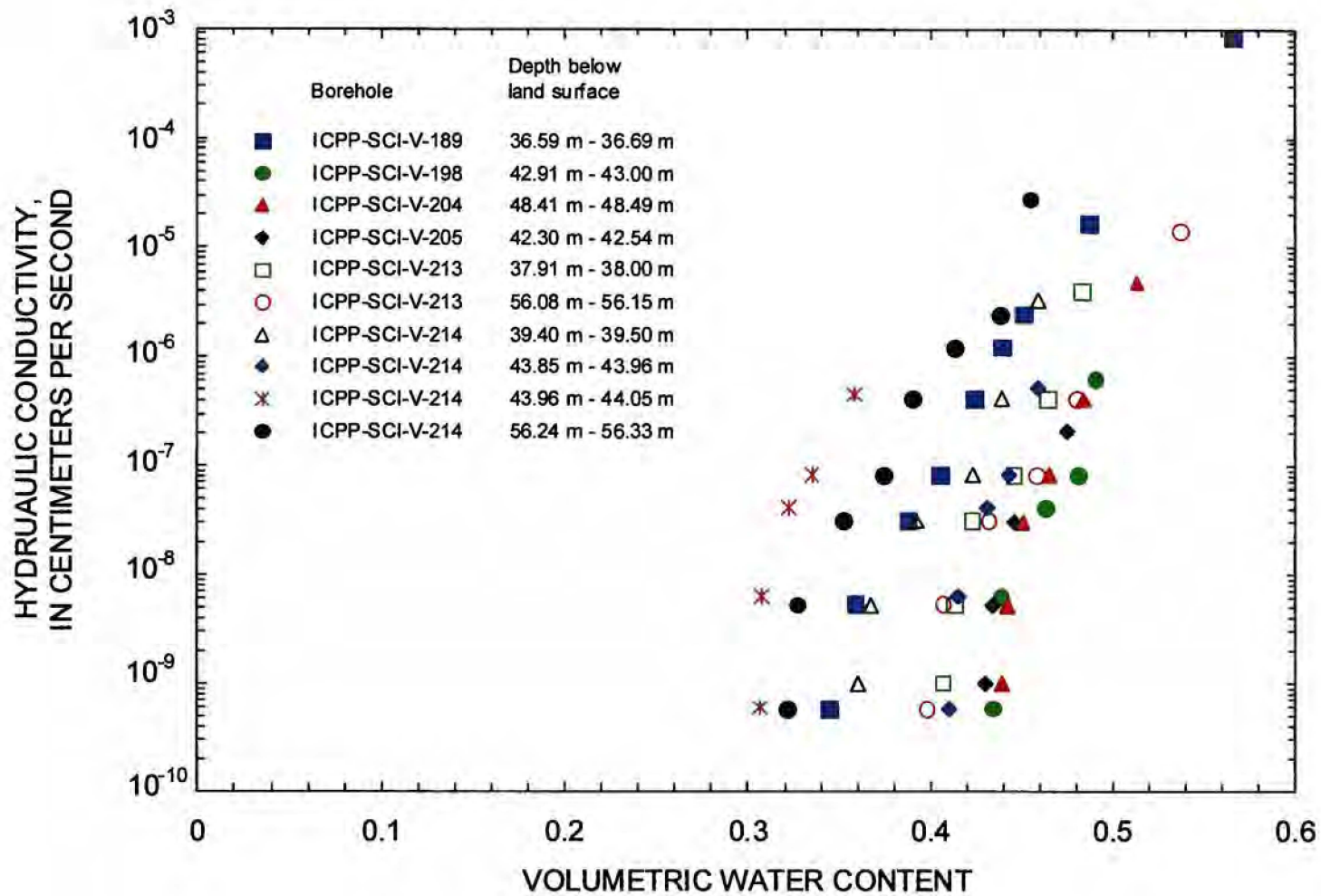
Figure 5. Hydraulic conductivity as a function of water content, measured using the steady-state centrifuge method, for 10 sedimentary interbed core samples collected from depths of 36.59 to 56.33 m below land surface within the Vadose Zone Research Park, Idaho National Engineering and Environmental Laboratory, Idaho.
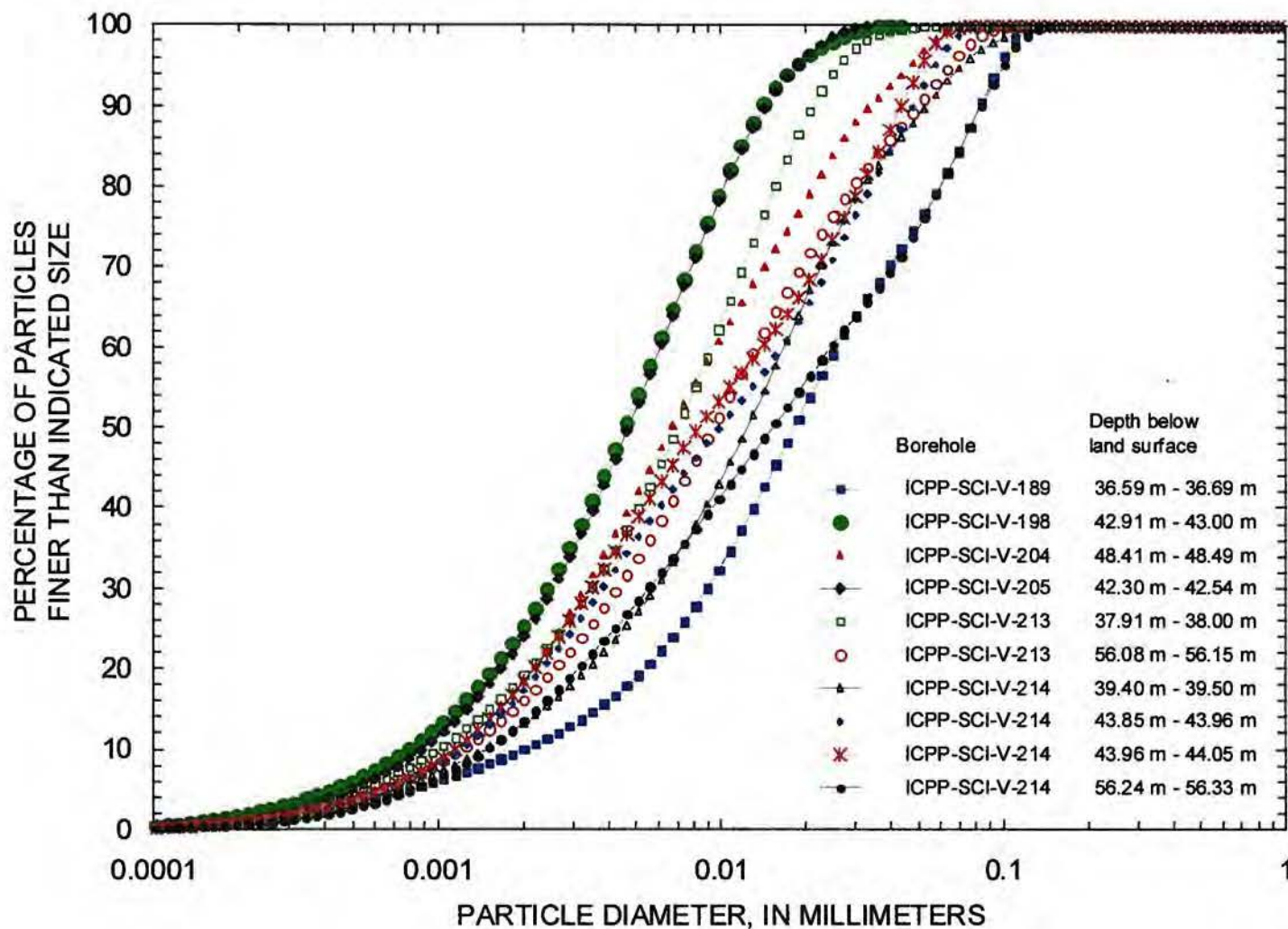
Figure 6. Cumulative particle-size distributions on a percent-finer-than basis for 10 sedimentary interbed core samples collected from depths of 36.59 to 56.33 m below land surface within the Vadose Zone Research Park, Idaho National Engineering and Environmental Laboratory, Idaho.

depths of approximately 35, 45, and 55 m below land surface. The 35-m interbed ranges in thickness from 0.6 to 8.5 m and is present in all of the 25 boreholes drilled to this depth or deeper. The 45-m interbed ranges from 0.6 to 10 m in thickness and is present in 6 (ICPP-SCI-V-189, -201A, -204, -205, -215, and ICPP-MON-V-212) of the 18 boreholes drilled to this depth or greater. The depth range for the 35- and 45-m interbeds tends to overlap due to local variations in the underlying basalt topography. The 55-m interbed ranges in thickness from 0.3 to 5 m and is encountered in 9 (ICPP-MON-A-165, -166, -167, ICPP-SCI-V-201, -209, ICPP-MON-V-212, ICPP-SCI-V-213, -214, and -215) of the 10 boreholes drilled to this depth or deeper. Thinner interbeds, ranging in thickness from 0.15 to 4.57 m, were noted in several of the holes from the drilling logs (Bechtel BWXT Idaho, LLC, 2002).

The 35-m interbed is laterally extensive to at least 900 m within the VZRP between the Big Lost River and the new percolation pond area. Because most boreholes were drilled to 50 m or less, it is difficult to make inferences about the lateral continuity of the 45- and 55-m interbeds.

Spatial variation of interbed properties

The geometric mean particle size and standard deviation for each of the 90 samples from this study and that of Perkins (2003) are plotted with adjusted depth in figures 7 and 8. Due to local variations in the topography of the underlying basalt flows and interbed thickness, the depths associated with each interbed vary slightly from hole to hole. In order to compare interbed properties between boreholes on an equal basis, the sample depths have been corrected to the tops of the interbed in a given hole. This was accomplished by subtracting the sample depth from the depth associated with the top of the interbed in each borehole (from the lithologic logs). Each of these numbers was then subtracted from the average starting depth of the respective interbed, defined at 35, 45, and 55 m. This approach effectively "straightens" the interbed highs and lows so that the top of each interbed lies on a horizontal plane. The bottom depth of each interbed varies depending on local interbed thicknesses. Each symbol represents the distance of a sample borehole from

ICPP-SCI-V-189 along cross section A-A' (shown in figure 3).

The textural variability within each interbed can be examined using figures 7 and 8. Vertically, the 35-m interbed is fairly uniform in geometric mean particle diameter and standard deviation, with the exception of samples from ICPP-SCI-V-214, which show more variation. The geometric mean particle diameter ranges from 0.0034 to 0.0160 mm, with the geometric standard deviation ranging from 2.8 to 4.6, indicating a moderately well-sorted material. Laterally, the particle-size statistics of the 35-m interbed vary little between boreholes at comparable sample depths. The 45-m interbed shows a coarsening upward trend, with the greatest spread in particle sizes near the top of the interbed. The geometric mean particle diameter ranges from 0.0038 to 0.1715 mm and the standard deviation varies from 2.8 to 8.3, increasing upward. The material from ICPP-SCI-V-215 is coarser and has a greater spread in particle sizes than that of ICPP-SCI-V-204, located approximately 240 m to the northwest. The 55-m interbed displays more variation in particle size vertically, with the mean ranging from 0.0081 to 0.1992 mm and the standard deviation ranging from 2.7 to 9.4. The sediment from ICPP-SCI-V-213 and ICPP-SCI-V-214 span similar ranges of mean particle size, while the sediment from ICPP-SCI-V-215 is coarser. Lateral heterogeneity within the 45- and 55-m interbeds is difficult to discern because few boreholes within the VZRP were drilled to these depths.

Textural differences between the 35-m, 45-m, and 55-m interbeds can be compared from the histograms presented in Figure 9, where the distributions of geometric mean particle diameter and standard deviation are plotted based on the number of samples analyzed per interbed. The 35-m interbed contains the finest material, with most of the samples plotting near the geometric mean particle diameter of 0.0042 mm. The 55-m interbed contains the coarsest material (up to 0.237 mm), with the largest frequency of samples having values near 0.0133 mm. The distribution of means from the 45-m interbed overlaps that of the other two.

17
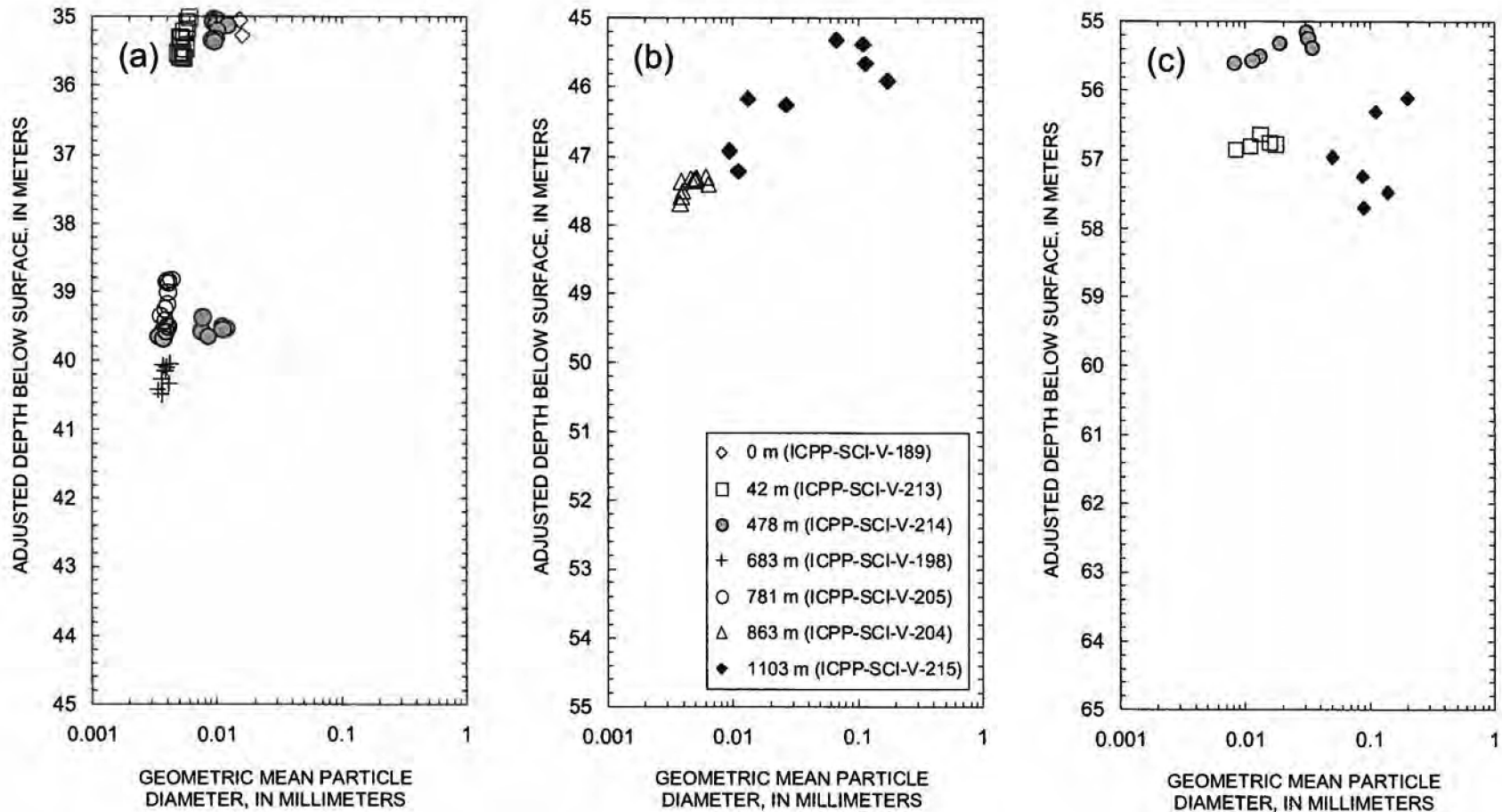
Figure 7. Geometric mean particle diameter for 90 samples (from this study and that of Perkins (2003)) plotted with depth below surface for (a) the 35-m interbed, (b) the 45-m interbed, and (c) the 55-m interbed. Depths were adjusted to the tops of the interbeds. Symbols represent the distances of sample boreholes (in parentheses) from ICPP-SCI-V-189 along cross section A-A' shown in figure 3.
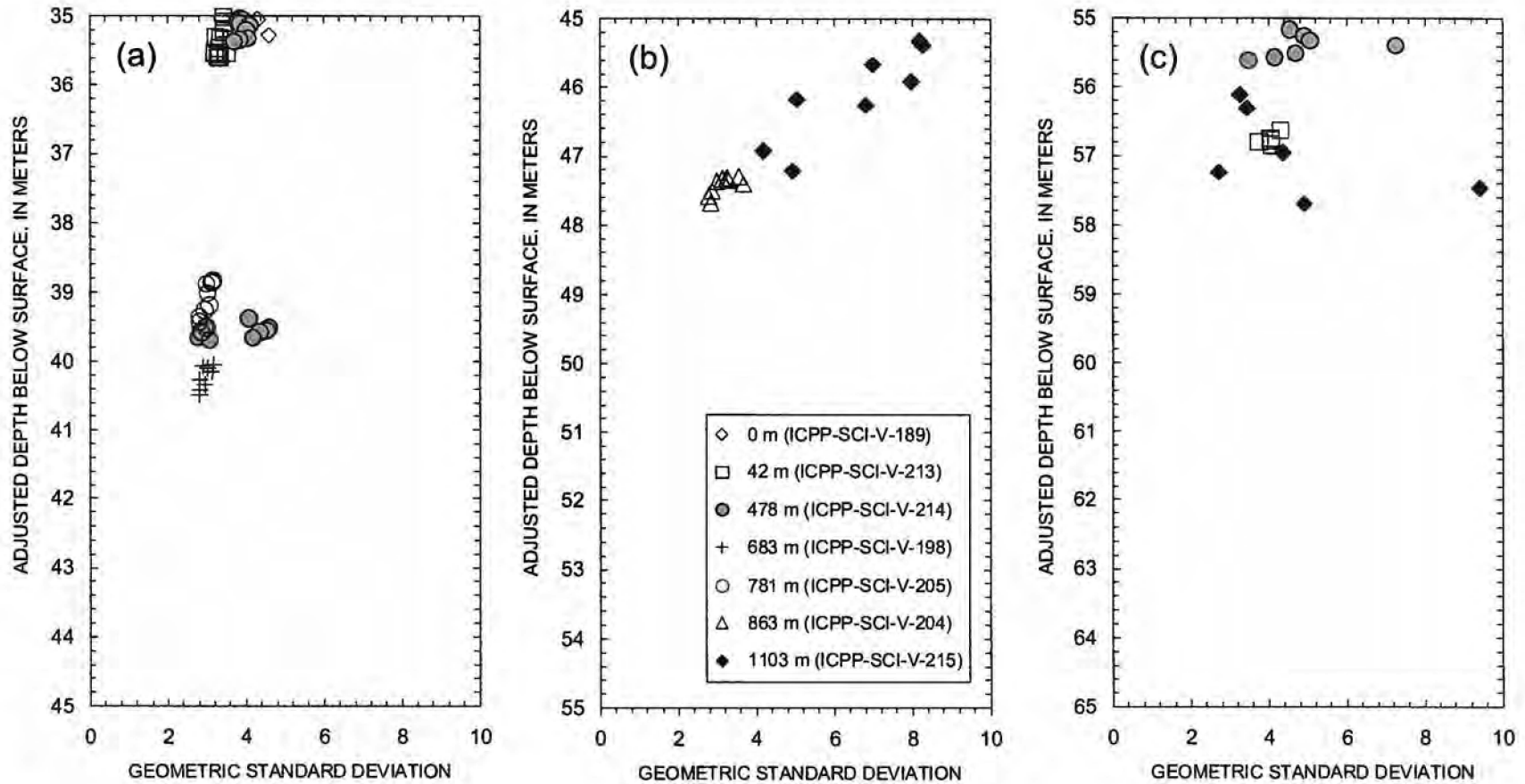
Figure 8. Geometric particle-size standard deviation for 90 samples (from this study and that of Perkins (2003)) plotted with depth below surface for (a) the 35-m interbed, (b) the 45-m interbed, and (c) the 55-m interbed. Depths were adjusted to the tops of the interbeds. Symbols represent distances of sample boreholes (in parentheses) from ICPP-SCI-V-189 along cross section A-A' shown in figure 3.
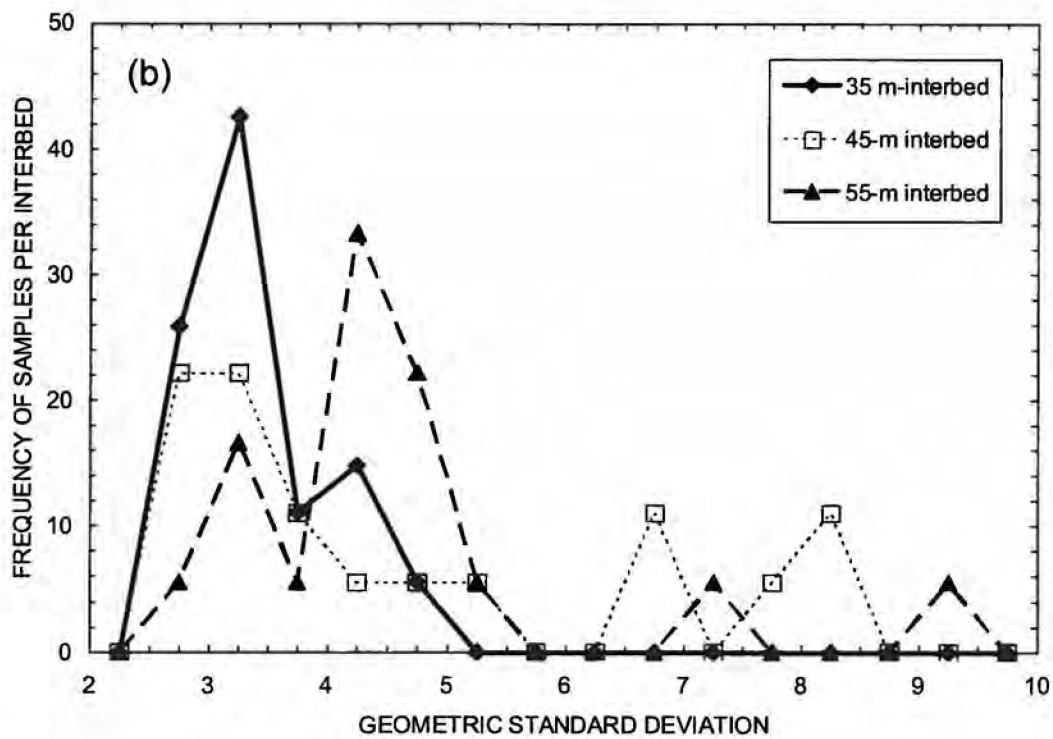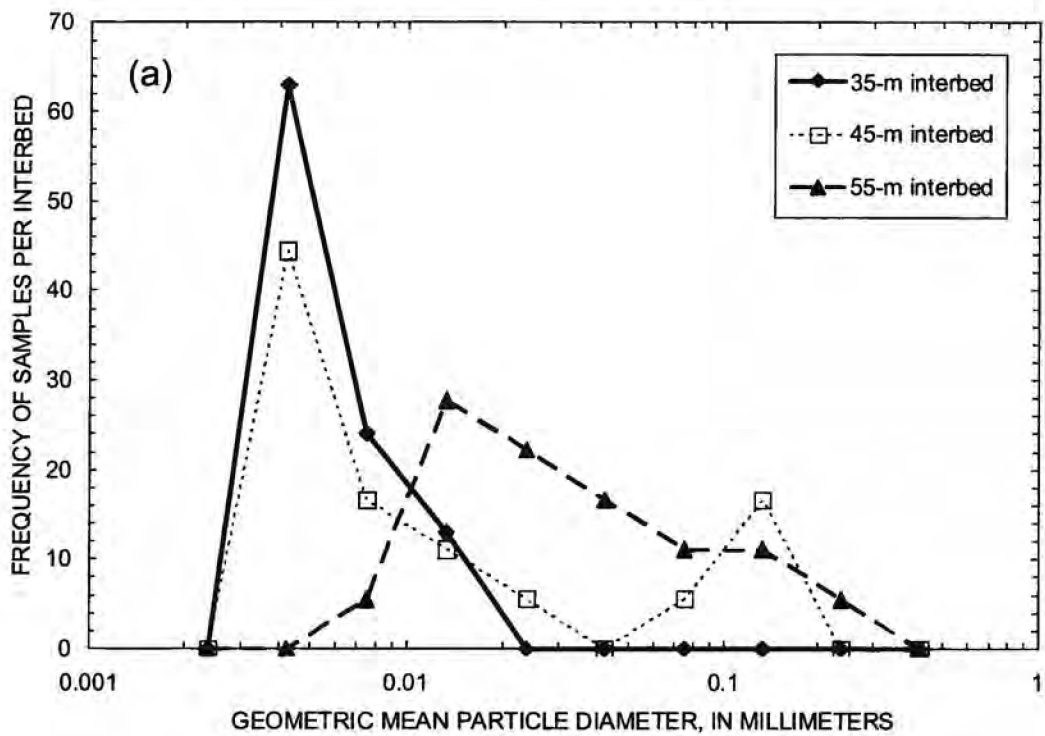
Figure 9. Frequency distribution of 90 samples (from this study and that of Perkins (2003)) within the 35-m, 45-m, and 55-m interbeds, based on (a) geometric mean particle diameter, and (b) geometric standard deviation.

Over the 1,100-m distance along the cross-section line A-A' (fig. 3), the geometric mean particle diameter and standard deviation vary little at the top and base of the 35-m interbed. The predominantly silt loam texture of this interbed and the relatively small values of geometric particle-size standard deviation suggest a low-energy depositional environment, possibly of floodplain or lacustrine origin. The 45-m interbed coarsens upward both locally (within ICPP-SCI-V-215) and over a distance of 200 m (between ICPP-SCI-V-204 and ICPP-SCI-V-215). Hughes (1993) interpreted coarsening upward sequences as being deposited by low-energy fluvial systems followed by higher energy fluvial systems, although the coarse layer here is comprised of sandy loam, not sand or gravel. The 55-m interbed shows the most textural variability, with no clear trend such as upward fining or coarsening. This may indicate more prominent depositional layering within this interbed, possibly from a braided fluvial environment. Bartholomay (1990) showed that the mineralogy of interbed sediments in the vicinity of the INTEC is similar to that of the modern Big Lost River deposits. Source areas and drainage patterns during interbed deposition may have been similar to those of the present day, suggesting that the silt-rich interbeds under the INTEC may be floodplain deposits of a river containing sediment similar to modern Big Lost River deposits.

Differences in particle size between the interbeds suggest that the hydraulic behavior of these interbeds will be different. Small-scale heterogeneity (less than a few meters) in the interbeds could enhance lateral flow or inhibit downward vertical flow depending on field water contents. Figure 10 shows saturated hydraulic conductivity, measured for the 22 core samples reported in this study and that of Perkins (2003), plotted with adjusted depth for each of the three interbeds. The K_{sat} values follow the same general trends as the particle size data. The 35-m interbed has K_{sat} values in the low to middle range of the spectrum with the exception of one sample with an anomalously high value of 8.31×10^{-4} cm/s. For the 45-m interbed, K_{sat} decreases with depth, consistent with the downward fining of particle size. For the 55-m interbed, K_{sat} generally increases with depth. This is consistent with the observed increase in the geometric mean particle size with depth. At low water contents, the presence of coarser sediment at the base of the 55-m interbed may promote lateral flow in the overlying fine interval. At higher water contents, this coarse-textured interval may act as a conduit for lateral flow along the underlying impermeable basalt interface or until fractures in the basalt are encountered. One implication of reduced permeability with depth is the possibility of water accumulating above a fine layer. The sedimentary intervals with the lowest K_{sat} values (10^{-7} cm/s) may cause the formation of perched water zones within or above the 35-, 45-, or 55-m interbeds.

Baked-zone intervals

Baked-zone intervals were identified qualitatively by their oxidized color and by their proximity to the tops of the interbeds. The oxidized color of the tops of the interbeds could be due to various factors, including the presence of organic material, the amount and type of iron, and whether water has leached iron out of the oxidized interval after basalt deposition. Most of the intervals defined as "baked" had basalt clasts present in the sediment or the actual basalt-sediment interface was observed through the transparent core liner. The fact that a distinct sediment color change occurs near the basalt interface seems to indicate that the intervals are baked, with the color likely varying because of other factors such as iron leaching, the form of iron in the original sediment (whether amorphous or not), and the amount of soil development. Also, the extent of baked-zone alteration depends on the temperature of the magma and the water content of the sediment during basalt deposition (Cecil and others, 1991).

After categorizing the material analyzed for particle size into initial color groups, each group was assigned a Munsell (1994) color (table 6). For hole ICPP-SCI-V-189, the top of a baked zone was identified from 36.59 to 37.04 m based on the reddish-yellow color (7.5YR 6/6). This 0.45-m interval represents a minimum thickness because material below 37.04 m was not analyzed. For hole ICPP-SCI-V-213, material from 37.50 to 38.11 m was also classified as reddish yellow (7.5YR 6/6). Material immediately above 37.50 m was not recovered during drilling and material

Figure 10. Saturated hydraulic conductivity for 22 core samples (from this study and that of Perkins (2003)) plotted with depth below land surface for (a) the 35-m interbed, (b) the 45-m interbed, and (c) the 55-m interbed. Depths were adjusted to the tops of the interbeds. Symbols represent the distance of the sample boreholes (in parentheses) from ICPP-SCI-V-189 along cross section A-A' shown in figure 3.
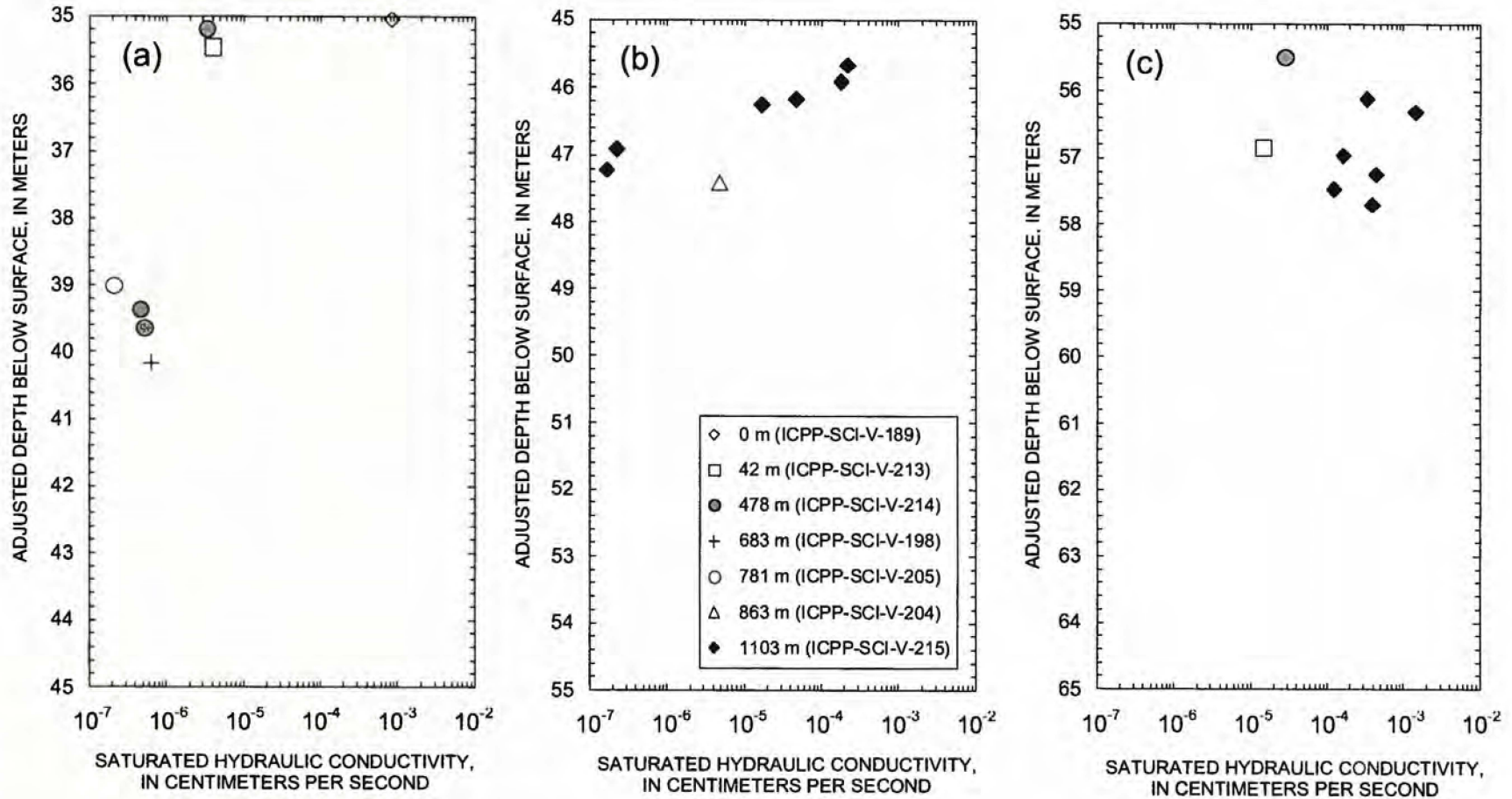
from 38.11 m to the base of the interbed at 42.07 m was not analyzed. The minimum baked-zone thickness is 0.61 m in this borehole for the 35-m interbed. For hole ICPP-SCI-V-214, a baked interval of yellowish-red color (5YR 5/6 to 5YR 5/8) exists from 55.94 to 56.03 m. Immediately below this interval, from 56.03 to 56.40 m, the material is light brown (7.5YR 6/4). It is likely that the baked zone extends from the top of the interbed at 55.79 to 56.03 m (with a maximum thickness equal to 0.24 m).

Baked sediment was not present at the top of every interbed studied. In hole ICPP-SCI-V-213, material from 55.79 to 56.14 m was light yellowish brown (10YR 6/4) to light brown (7.5YR 6/4). The top of the interbed occurs at 55.09 m according to the lithologic log (Bechtel BWXT Idaho, LLC, 2002), so there is potentially 0.7 m of baked material overlying the interval studied. In hole ICPP-SCI-V-214, the material analyzed from the top of the interbed at 39.26 m to a depth of 39.63 m is very pale brown (10YR 7/3). Lower in the same interbed, from 43.75 to 44.36 m, the sediment is also very pale brown.

Baked-zone material was studied for the 45- and 55-m interbeds in borehole ICPP-SCI-V-215 by Perkins (2003). Munsell (1994) colors for this borehole were not described by Perkins (2003), but are assigned here. The material in the 45-m interbed grades from reddish yellow (7.5YR 6/6) to light brown (7.5YR 6/4) with increasing depth, with the baked interval occurring from 45.53 to 45.95 m. The top of the interbed occurs at 45.24 m according to the visual lithologic log (Linda Davis, USGS, personal commun., 2003), making the maximum thickness of this baked interval 0.71 m. The material in the 55-m interbed changes from red (2.5YR 5/6) to brown (7.5YR 5/4) with increasing depth. The baked interval occurs from 58.36 to 59.30 m, based on the material studied. The maximum thickness, with the top of the interbed starting at 57.29 m in the visual lithologic log, is 2.01 m.

Table 6 compares the average particle-size statistics (geometric mean and standard deviation) for baked and non-baked intervals based on the number of samples indicated in the last column. In general, there is no distinct particle-size differ-ence between baked-zone material and the underlying non-baked sediment. There is lateral variation in particle size between baked intervals. The baked zone of the 55-m interbed of ICPP-SCI-V-215 is coarser than the baked zone for the same interbed in ICPP-SCI-V-214, and the baked zone of the 35-m interbed in ICPP-SCI-V-189 is coarser than that for the same interbed in ICPP-SCI-V-213. The average geometric particle-size standard deviation ranges from 2.95 to 5.79 for non-baked sediment and ranges from 3.34 to 7.82 for baked sediment for all interbeds and boreholes, with the largest standard deviations occurring in the 45-m interbed of ICPP-SCI-V-215.

Figure 11 compares $\theta(\psi)$ and $K(\theta)$ curves measured on cores from baked-zone intervals identified in ICPP-SCI-V-189 and ICPP-SCI-V-213 (from this study) and from ICPP-SCI-V-215 (Perkins, 2003). Strong aggregation due to clay coatings on particles was observed within the baked zone of the 45-m interbed of ICPP-SCI-V-215 (Perkins, 2003); no aggregation was observed in the baked-zone intervals of the 35- or 55-m interbeds. Any structural influences on the hydraulic properties due to aggregation are subtle compared to the textural influences. The cores group by texture with the coarsest samples occurring in the baked zone of the 55-m interbed of ICPP-SCI-V-215 and the finest samples in the baked zones of the 35-m interbed in holes ICPP-SCI-V-189 and ICPP-SCI-V-213.

SUMMARY

Three relatively thick interbeds, starting at depths of approximately 35, 45, and 55 m below land surface, were identified from 32 boreholes drilled within the VZRP. The 35-m interbed is laterally extensive to at least 900 m within the VZRP between the Big Lost River and the new percolation pond area for the INTEC facility. Not enough information was available, due to limited borehole completion depths, to infer the lateral extent of the 45- and 55-m interbeds. The majority of the samples analyzed in this study were classified as silt loams. The 35-m interbed contained the finest samples, with an average geometric mean particle size of 0.0063 mm based on 54 samples, while the 55-m interbed had the coarsest material with an
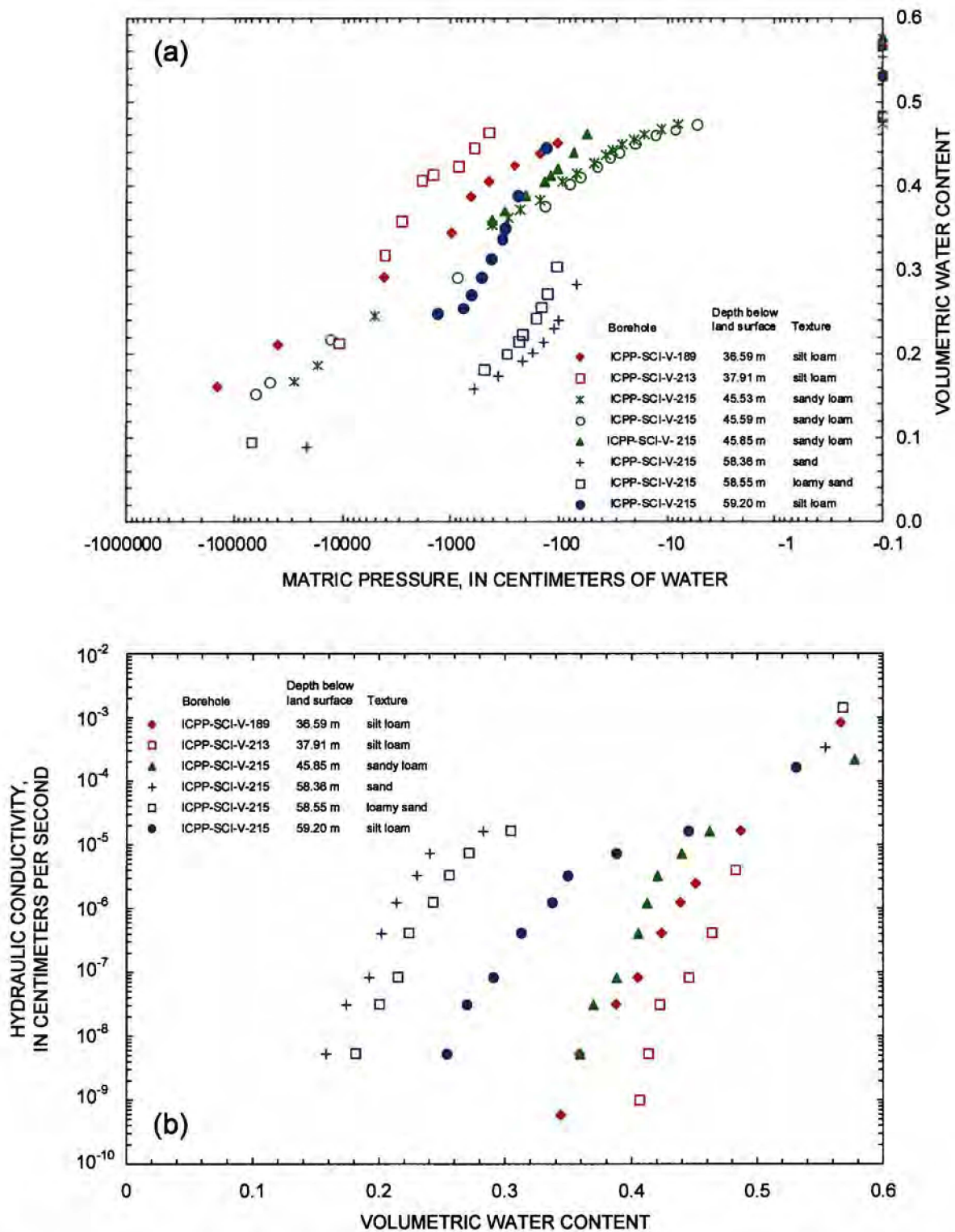
Figure 11. Comparison of unsaturated hydraulic properties measured on core samples (from this study and that of Perkins (2003)) from baked-zone intervals defined in the 35-m (red symbols), 45-m (green), and 55-m (blue) interbeds. (a) water content as a function of matric pressure, or water retention. (b) hydraulic conductivity as a function of water content.

24

average geometric mean particle size of 0.0494 mm based on 18 samples. The average geometric mean particle size of the 45-m interbed was 0.0316 mm, based on 18 samples. The 35-m interbed was the most uniform texturally, both vertically and laterally over the 900 m range studied. The 45-m interbed coarsened upward vertically, with the coarsest material located near the new percolation pond area. The 55-m interbed showed more variation in particle size with depth.

Saturated hydraulic conductivity values ranged from 1.66×10^{-7} to 1.42×10^{-3} cm/s for the 10 samples from this study and the 12 samples from ICPP-SCI-V-215 (Perkins, 2003). For six samples from the 35-m interbed (excluding one sample with an anomalously high value), the average K_{sat} was 1.525×10^{-6} cm/s and the average porosity was 0.4678. For the 45-m interbed, the average K_{sat} was 6.67×10^{-5} cm/s for seven samples and the average porosity was 0.4963 based on nine samples. The average K_{sat} for the 55-m interbed was 3.644×10^{-4} cm/s and the porosity was 0.5144 for eight samples. Low permeability intervals (with K_{sat} values of 10^{-7} cm/s or less) within the 35- and 45-m interbeds may cause perched water zones to form, and promote lateral flow within the overlying, more coarsely textured sediment intervals or rubble zones at basalt-sediment interfaces.

Baked zones were identified at the tops of the (1) 35-m interbed, in holes ICPP-SCI-V-189 and ICPP-SCI-V-213, (2) 45-m interbed, in ICPP-SCI-V-215, and (3) 55-m interbed, in holes ICPP-SCI-V-214 and ICPP-SCI-V-215. The average geometric mean particle diameter for these baked intervals did not differ significantly from that of the underlying non-baked intervals. Available hydraulic property data, from this study and from Perkins (2003), were compared for these intervals. Although aggregation was observed for cores from the 45-m interbed in ICPP-SCI-V-215, the effect on the hydraulic properties was subtle when compared to textural influences. Therefore, the hydraulic properties of baked-zone intervals are not likely to differ significantly from non-baked intervals except as affected by texture.

Beneath the old percolation ponds near the INTEC, perched water zones were observed to form presumably as a result of reduced permeabil-ity layers at depth and the high inputs of water to the ponds. Reduced permeability zones in the 35-, 45-, and 55-m interbeds, based on analyses presented in this study, may contribute to perching below the new percolation pond area. If large inputs of water are applied to the ponds or large amounts of water from the nearby Big Lost River infiltrate the subsurface, mounding of perched water can contribute to lateral flow—a potential mechanism for contaminant transport away from the new percolation ponds.

REFERENCES CITED

Anderson, S.R., 1991, Stratigraphy of the unsaturated zone and uppermost part of the Snake River Plain aquifer at the Idaho Chemical Processing Plant and Test Reactors Area, Idaho National Engineering Laboratory, Idaho: U.S. Geological Survey Water-Resources Investigations Report 91–4010 (DOE/ID–22095), 71 p.

Anderson, S.R., Liszewski, M.J., and Ackerman, D.J., 1996, Thickness of surficial sediment at and near the Idaho National Engineering Laboratory, Idaho: U.S. Geological Survey Open-File Report 96–330 (DOE/ID–22128), 16 p.

Arya, L.M., and Paris, J.F., 1981, A physicoempir-ical model to predict the soil moisture characteristic from particle-size distribution and bulk density data: Soil Science Society of America Journal, v. 45, p. 1023–1030.

Barraclough, J.T., Lewis, B.D., and Jensen, R.G., 1981, Hydrologic conditions at the Idaho National Engineering Laboratory, Idaho; emphasis 1974–1978: U.S. Geological Survey Water-Supply Paper W2191, 52 p.

Bartholomay, R.C., 1990, Mineralogical correlation of surficial sediment from area drainages with selected sedimentary interbeds at the Idaho National Engineering Laboratory, Idaho: U.S. Geological Survey Water-Resources Investigations Report 90–4147 (DOE/ID–22092), 18 p.

Bartholomay, R.C., Tucker, B.J., Ackerman, D.J., and Liszewski, M.J., 1997, Hydrologic conditions and distribution of selected radiochemi-

cal and chemical constituents in water, Snake River Plain aquifer, Idaho National Engineering Laboratory, Idaho, 1992 through 1995: U.S. Geological Survey Water-Resources Investigations Report 97–4086, 57 p.

Bartholomay, R.C., 1998, Distribution of selected radiochemical and chemical constituents in perched ground water, Idaho National Engineering Laboratory, Idaho, 1992–95: U.S. Geological Survey Water Resources Investigations Report 98–4026 (DOE/ID–22145), 59 p.

Bechtel BWXT Idaho, LLC, 2002, Vadose zone instrumented well and borehole installations near the new INTEC percolation pond area end of well reports: Idaho National Engineering and Environmental Laboratory, Environmental Restoration Directorate Report INEEL/EXT–02–00085, [variously paged].

Bechtel BWXT Idaho, LLC, 2003, INEEL Vadose Zone Research Park, accessed February 27, 2003 at http://www.inel.gov/env-energy-science/geo/vz_park.shtml.

Beyer, W.H., ed., 1991, CRC Standard Mathematical Tables and Formulae (29th ed.): CRC Press, Inc., Boca Raton, Florida, 609 p.

Blake, G.R., and Hartge, K.H., 1986, Particle density, in Klute, A., ed., Methods of Soil Analysis, Part I-Physical and Mineralogical Methods (2nd ed.): Soil Science Society of America Agronomy Monograph, n. 9, Madison, Wisconsin, p. 378–379.

Brunauer, S., Emmett, P.H., and Teller, E., 1938, Adsorption of gases in multimolecular layers: Journal of the American Chemical Society, v. 60, p. 309–319.

Cecil, L.D., Orr, B.R., Norton, T., and Anderson, S.R., 1991, Formation of perched ground-water zones and concentrations of selected chemical constituents in water, Idaho National Engineering Laboratory, Idaho 1986–88: U.S. Geological Survey Water Resources Investigations Report 91–4166, 53 p.

Chandler, R.J., and Gutierrez, C.I., 1986, The filter-paper method of suction measurement: Geotechnique, v. 36, p. 265–268.

Conca, J.L., and Wright, J.V., 1998, The UFA method for rapid, direct measurements of unsaturated transport properties in soil, sediment, and rock: Australian Journal of Soil Research, v. 36, p. 291–315.

Fawcett, R.G., and Collis-George, N., 1967, A filter paper method for determining the moisture characteristics of soil: Australian Journal of Experimental Agriculture and Animal Husbandry, v. 7, n. 24, p. 162–167.

Gee, G.W., and Or, D., 2002, Laser light scattering (diffraction) [particle-size analysis], in Dane, J.H., and Topp, G.C., eds., Methods of Soil Analysis, Part 4—Physical Methods: Soil Science Society of America Book Series, n. 5, Madison, Wisconsin, p. 286–293.

Greacen, E.L., Walker, G.R., and Cook, P.G., 1987, Evaluation of the filter paper method for measuring soil water suction: International Conference on Measurement of Soil and Plant Water Status, v. 1, p. 137–143.

Hackett, B., Pelton, J., and Brockway, C., 1986, Geohydrologic story of the eastern Snake River Plain and the Idaho National Engineering Laboratory: U.S. Department of Energy, Idaho Operations Office, Idaho National Engineering Laboratory, 32 p.

Hamblin, A.P., 1981, Filter-paper method for routine measurement of field water potential: Journal of Hydrology, v. 53, p. 355–360.

Hughes, J.D., 1993, Analysis of characteristics of sedimentary interbeds at the Radioactive Waste Management Complex, Idaho National Engineering Laboratory, Idaho: Idaho State University at Pocatello, M.S. thesis, 74 p.

Klute, A., and Dirksen, C., 1986, Hydraulic conductivity and diffusivity: laboratory methods, in Klute, A., ed., Methods of Soil Analysis, Part I—Physical and Mineralogical Methods (2nd ed.): Soil Science Society of America Agronomy Monograph, n. 9, Madison, Wisconsin, p. 687–732.

Liszewski, M.J., and Mann, L.J., 1992, Purgeable organic compounds in ground water at the Idaho National Engineering Laboratory, Idaho—1990 and 1991: U.S. Geological Survey Open-File Report 92–174, 19 p.

Miller, E.E., and Miller, R.D., 1956, Physical theory for capillary flow phenomena: Journal of Applied Physics, v. 27, p. 324–332.

Miller, E.E., 1980, Similitude and scaling of soil-water phenomena, in Hillel, D., ed., Applications of Soil Physics: Academic Press, New York, p. 300–318.

Munsell Color, 1994, Munsell soil color charts (revised edition): GretagMacbeth, New Windsor, New York, [variously paged].

Nimmo, J.R., and Mello, K.A., 1991, Centrifugal techniques for measuring saturated hydraulic conductivity: Water Resources Research, v. 27, p. 1263–1269.

Nimmo, J.R., Stonestrom, D.A., and Akstin, K.C., 1994, The feasibility of recharge rate determinations using the steady-state centrifuge method: Soil Science Society of America Journal, v. 58, p. 49–56.

Nimmo, J.R., Deason, J.A., Izbicki, J.A., and Martin, P., 2002a, Evaluation of unsaturated-zone water fluxes in heterogeneous alluvium at a Mojave Basin site: Water Resources Research, v. 38, n. 10, p. 33-1 to 33-13.

Nimmo, J.R., Perkins, K.S., and Lewis, A.M., 2002b, Steady-state centrifuge [simultaneous determination of water transmission and retention properties], in Dane, J.H., and Topp, G.C., eds., Methods of Soil Analysis, Part 4—Physical methods: Soil Science Society of America Book Series, n. 5, Madison, Wisconsin, p. 903–916, 1041–1045.

Perkins, K.S., 2003, Measurement of sedimentary interbed hydraulic properties and their hydrologic influence near the Idaho Nuclear Technology and Engineering Center at the Idaho National Engineering and Environmental Laboratory: U.S. Geological Survey Water-Resources Investigations Report 03–4048, 19 p.

Schaap, M., 1999, Rosetta model version 1.0, accessed March 13, 2003 at http://www.ussl.ars.usda.gov/models/rosetta/rosetta.HTM.

Soil Survey Staff, 1975, Soil taxonomy: A basic system of soil classification for making and interpreting soil surveys: USDA-SCS Agriculture Handbook n. 436, U.S. Government Printing Office, Washington, DC, 754 p.

van Genuchten, M.Th., 1980, A closed-form equation for predicting the hydraulic conductivity of unsaturated soils: Soil Science Society of America Journal, v. 44, p. 892-898.

Webb, P.A., and Orr, C., 1997, Analytical methods in fine particle technology: Micromeritics Instrument Corporation, Norcross, Georgia, 301 p.

Table 1. Measured values of bulk density, particle density, and porosity for 10 core samples

[Initial bulk density (ρ_{bi}) and porosity (Φ_i) values represent the state of the samples after re-coring them for the steady-state centrifuge method, prior to centrifugation. Final values (ρ_{bf} and Φ_f) were calculated after the completion of all centrifuge and matric pressure measurements. Particle density (ρ_s) was measured on excess material saved during sample re-coring.]

Borehole	Depth interval (m)	Particle density, ρ_s (g/cm^3)	Initial bulk density, ρ_{bi} (g/cm^3)	Final bulk density, ρ_{bf} (g/cm^3)	Initial total porosity, Φ_i (cm^3/cm^3)	Final total porosity, Φ_f (cm^3/cm^3)
ICPP-SCI-V-189	36.59–36.69	2.74	1.18	1.19	0.5705	0.5661
ICPP-SCI-V-198	42.91–43.00	2.80	1.41	1.53	0.4972	0.4553
ICPP-SCI-V-204	48.41–48.49	2.84	1.35	1.39	0.5244	0.5096
ICPP-SCI-V-205	42.30–42.54	2.80	1.44	1.50	0.4872	0.4642
ICPP-SCI-V-213	37.91–38.00	2.77	1.38	1.54	0.5028	0.4444
ICPP-SCI-V-213	56.08–56.15	2.80	1.25	1.40	0.5528	0.5014
ICPP-SCI-V-214	39.40–39.50	2.74	1.49	1.60	0.4575	0.4156
ICPP-SCI-V-214	43.85–43.96	2.78	1.51	1.53	0.4562	0.4499
ICPP-SCI-V-214	43.96–44.05	2.74	1.63	1.63	0.4061	0.4061
ICPP-SCI-V-214	56.24–56.33	2.82	1.48	1.71	0.4755	0.3944

Table 2. Saturated hydraulic conductivity determined by the falling-head method and the associated saturated water content for 10 core samples

[For some samples, an alternative version of the standard falling-head method, using a centrifuge, was implemented to measure saturated hydraulic conductivity (K_{sat}). Abbreviations: S = the standard application (gravity driven only); C = a centrifuge was used to increase the driving force for flow (in addition to gravity).]

Borehole	Depth interval (m)	Saturated hydraulic conductivity, K_{sat} (cm/s)	Method	Saturated water content, θ_{sat} (cm^3/cm^3)
ICPP-SCI-V-189	36.59–36.69	8.31×10^{-4}	S	0.5661
ICPP-SCI-V-198	42.91–43.00	6.35×10^{-7}	S	0.4904
ICPP-SCI-V-204	48.41–48.49	4.80×10^{-6}	S	0.5134
ICPP-SCI-V-205	42.30–42.54	2.07×10^{-7}	C	0.4752
ICPP-SCI-V-213	37.91–38.00	3.99×10^{-6}	C	0.4829
ICPP-SCI-V-213	56.08–56.15	1.44×10^{-5}	S	0.5368
ICPP-SCI-V-214	39.40–39.50	3.34×10^{-6}	C	0.4591
ICPP-SCI-V-214	43.85–43.96	5.20×10^{-7}	C	0.4593
ICPP-SCI-V-214	43.96–44.05	4.59×10^{-7}	C	0.3585
ICPP-SCI-V-214	56.24–56.33	2.81×10^{-5}	S	0.4546

Table 3. Unsaturated hydraulic property measurements for 10 core samples

[The first values listed for each sample are the saturated values of water content (θ) and hydraulic conductivity (K), assuming the matric pressure (ψ) is -0.1 cm-water. Saturated water contents were determined using initial volumes calculated prior to centrifugation; subsequently drier water contents were calculated using the final sample volume determined after centrifugation. A tensiometer was generally used for the pressure range > -700 cm-water; the filter paper method was used for the range < -700 cm-water. Abbreviations: T = tensiometer; F = filter paper method; ND = not determined; A = assumed.]

Borehole	Depth interval (m)	Matric pressure, ψ (cm-water)	Method	Water content, θ (cm^3/cm^3)	Hydraulic conductivity, K (cm/s)
ICPP-SCI-V-189	36.59–36.69	-0.10	A	0.5661	8.31×10^{-4}
		ND		0.4869	1.66×10^{-5}
		-103.36	T	0.4509	2.49×10^{-6}
		-150.83	T	0.4389	1.24×10^{-6}
		-254.66	T	0.4239	4.15×10^{-7}
		-450.17	T	0.4051	8.29×10^{-8}
		-646.77	T	0.3877	3.14×10^{-8}
		ND		0.3590	5.31×10^{-9}
		-989.83	F	0.3442	5.84×10^{-10}
		-4,206.87	F	0.2916	ND
		-40,418.04	F	0.2112	ND
		-144,436.53	F	0.1610	ND
ICPP-SCI-V-198	42.91–43.00	-0.10	A	0.4904	6.35×10^{-7}
		-283.84	T	0.4810	8.33×10^{-8}
		-429.60	T	0.4635	4.17×10^{-8}
		-1,471.36	F	0.4388	6.30×10^{-9}
		-1,567.72	F	0.4343	5.87×10^{-10}
		-4,998.58	F	0.3936	ND
		-7,474.01	F	0.3549	ND
		-25,827.87	F	0.2430	ND
ICPP-SCI-V-204	48.41–48.49	-0.10	A	0.5134	4.80×10^{-6}
		-182.47	T	0.4839	4.08×10^{-7}
		ND		0.4651	8.16×10^{-8}
		-731.63	F	0.4506	3.09×10^{-8}
		-1,362.38	F	0.4419	5.22×10^{-9}
		-1,575.27	F	0.4390	9.93×10^{-10}

Table 3. Unsaturated hydraulic property measurements for 10 core samples—Continued

Borehole	Depth interval (m)	Matric pressure, ψ (cm-water)	Method	Water content, θ (cm^3/cm^3)	Hydraulic conductivity, K (cm/s)
ICPP-SCI-V-204	48.41–48.49	-4,087.46	F	0.3767	ND
		-5,477.04	F	0.3291	ND
		-30,020.44	F	0.2259	ND
ICPP-SCI-V-205	42.30–42.54	-0.10	A	0.4752	2.07×10^{-7}
		-749.46	F	0.4457	3.09×10^{-8}
		-1,700.01	F	0.4344	5.22×10^{-9}
		-2,372.78	F	0.4300	9.93×10^{-10}
		-5,866.91	F	0.3658	ND
		-8,648.10	F	0.3063	ND
		-40,517.24	F	0.2192	ND
ICPP-SCI-V-213	37.91–38.00	-0.10	A	0.4829	3.99×10^{-6}
		-440.15	T	0.4643	4.13×10^{-7}
		-605.01	F	0.4459	8.26×10^{-8}
		-846.96	F	0.4227	3.12×10^{-8}
		-1,467.96	F	0.4136	5.28×10^{-9}
		-1,857.58	F	0.4067	1.00×10^{-9}
		-2,876.28	F	0.3584	ND
		-4,107.16	F	0.3179	ND
		-10,973.00	F	0.2131	ND
ICPP-SCI-V-213	56.08–56.15	-0.10	A	0.5368	1.44×10^{-5}
		-279.29	T	0.4801	4.14×10^{-7}
		-587.02	T	0.4581	8.28×10^{-8}
		-770.85	T	0.4317	3.13×10^{-8}
		ND		0.4066	5.30×10^{-9}
		-1,295.02	F	0.3979	5.83×10^{-10}
		-2,678.79	F	0.3567	ND
		-7,536.91	F	0.2565	ND
		-109,289.94	F	0.1551	ND
ICPP-SCI-V-214	39.40–39.50	-0.10	A	0.4591	3.34×10^{-6}
		-587.06	T	0.4389	4.10×10^{-7}
		-584.82	F	0.4229	8.20×10^{-8}

Table 3. Unsaturated hydraulic property measurements for 10 core samples—Continued

Borehole	Depth interval (m)	Matric pressure, ψ (cm-water)	Method	Water content, θ (cm^3/cm^3)	Hydraulic conductivity, K (cm/s)
ICPP-SCI-V-214	39.40–39.50	-720.82	F	0.3923	3.10×10^{-8}
		-1,235.10	F	0.3670	5.25×10^{-9}
		-1,320.56	F	0.3600	9.97×10^{-10}
		-3,231.76	F	0.2977	ND
		-4,694.39	F	0.2378	ND
		-52,761.10	F	0.1720	ND
ICPP-SCI-V-214	43.85–43.96	-0.10	A	0.4593	5.20×10^{-7}
		-362.39	T	0.4433	8.35×10^{-8}
		-488.54	T	0.4314	4.18×10^{-8}
		-1,094.35	F	0.4150	6.32×10^{-9}
		-998.40	F	0.4106	5.88×10^{-10}
		-6,109.27	F	0.3560	ND
		-30,815.11	F	0.2755	ND
		-82,632.24	F	0.2315	ND
ICPP-SCI-V-214	43.96–44.05	-0.10	A	0.3585	4.59×10^{-7}
		-252.12	T	0.3350	8.40×10^{-8}
		-495.23	T	0.3228	4.20×10^{-8}
		-689.52	F	0.3079	6.35×10^{-9}
		-605.87	F	0.3069	5.91×10^{-10}
		-3,948.63	F	0.2646	ND
		-10,605.80	F	0.2162	ND
		-22,685.76	F	0.1663	ND
ICPP-SCI-V-214	56.24–56.33	-0.10	A	0.4546	2.81×10^{-5}
		-0.88	T	0.4383	2.47×10^{-6}
		-196.50	T	0.4133	1.24×10^{-6}
		-433.78	T	0.3907	4.12×10^{-7}
		-569.00	T	0.3744	8.23×10^{-8}
		-641.66	T	0.3523	3.11×10^{-8}
		-815.72	F	0.3272	5.27×10^{-9}
		-1,361.23	F	0.3215	5.80×10^{-10}

Table 3. Unsaturated hydraulic property measurements for 10 core samples—Continued

Borehole	Depth interval (m)	Matric pressure, ψ (cm-water)	Method	Water content, θ (cm^3/cm^3)	Hydraulic conductivity, K (cm/s)
ICPP-SCI-V-214	56.24–56.33	-2,635.72	F	0.2795	ND
		-4,663.04	F	0.2365	ND
		-71,395.14	F	0.1533	ND

Table 4. Textural class percentages and nomenclature using the U.S. Department of Agriculture's soil classification system for 76 bulk and core samples

[Textural class percentages are calculated as the weight of sediment (g) in a given textural class, or particle-size interval (in mm), divided by the total weight of sediment (g) analyzed. The textural class name is determined graphically from the U.S. Department of Agriculture's textural triangle and reflects the relative proportions of gravel, sand, silt, and clay in a sample.l

Borehole	Depth interval (m)	Gravel (> 2 mm) (%)	Sand (2-0.05 mm) (%)	Silt (0.05-0.002 mm) (%)	Clay (< 0.002 mm) (%)	Texture
ICPP-SCI-V-189	36.59–36.69	0.00	23.19	66.85	9.94	silt loam
ICPP-SCI-V-189	36.69–37.04	0.00	26.41	63.61	9.95	silt loam
ICPP-SCI-V-198	42.84–42.86	0.00	0.00	76.25	23.72	silt loam
ICPP-SCI-V-198	42.86–42.89	0.00	0.00	73.64	26.38	silt loam
ICPP-SCI-V-198	42.89–42.91	0.00	0.00	75.39	24.63	silt loam
ICPP-SCI-V-198	42.91–43.00	0.00	0.00	74.81	25.21	silt loam
ICPP-SCI-V-198	43.05–43.06	0.00	0.00	73.83	26.17	silt loam
ICPP-SCI-V-198	43.13–43.14	0.00	0.00	75.93	24.08	silt loam
ICPP-SCI-V-198	43.22–43.24	0.00	0.00	72.48	27.51	silty clay loam
ICPP-SCI-V-198	43.28–43.29	0.00	0.00	72.93	27.06	silty clay loam
ICPP-SCI-V-204	48.32–48.35	0.00	2.10	79.74	18.12	silt loam
ICPP-SCI-V-204	48.35–48.36	0.00	0.01	78.97	21.05	silt loam
ICPP-SCI-V-204	48.36–48.37	0.00	0.48	76.28	23.25	silt loam
ICPP-SCI-V-204	48.37–48.38	0.00	0.69	77.12	22.20	silt loam
ICPP-SCI-V-204	48.38–48.39	0.00	0.00	78.27	21.74	silt loam
ICPP-SCI-V-204	48.39–48.41	0.00	0.00	73.87	26.16	silt loam
ICPP-SCI-V-204	48.41–48.49	0.00	3.16	78.46	18.43	silt loam
ICPP-SCI-V-204	48.54–48.55	0.00	0.00	75.37	24.64	silt loam
ICPP-SCI-V-204	48.62–48.63	0.00	0.00	74.83	25.20	silt loam
ICPP-SCI-V-204	48.70–48.74	0.00	0.00	73.8	26.21	silt loam
ICPP-SCI-V-205	42.23–42.24	0.00	0.00	76.89	23.16	silt loam
ICPP-SCI-V-205	42.24–42.26	0.00	0.00	75.52	24.52	silt loam
ICPP-SCI-V-205	42.26–42.27	0.00	0.00	76.22	23.71	silt loam
ICPP-SCI-V-205	42.27–42.30	0.00	0.00	76.38	23.65	silt loam
ICPP-SCI-V-205	42.30–42.54	0.00	0.00	76.06	23.97	silt loam
ICPP-SCI-V-205	42.59–42.61	0.00	0.00	75.43	24.59	silt loam
ICPP-SCI-V-205	42.66–42.67	0.00	0.00	75.37	24.67	silt loam
ICPP-SCI-V-205	42.75–42.76	0.00	0.00	73.74	26.26	silt loam
ICPP-SCI-V-205	42.83–42.84	0.00	0.00	75.07	24.92	silt loam
ICPP-SCI-V-205	42.91–42.92	0.00	0.00	76.29	23.68	silt loam

33

Table 4. Textural class percentages and nomenclature using the U.S. Department of Agriculture's soil classification system for 76 bulk and core samples—Continued

Borehole	Depth interval (m)	Gravel (> 2 mm) (%)	Sand (2-0.05 mm) (%)	Silt (0.05-0.002 mm) (%)	Clay (< 0.002 mm) (%)	Texture
ICPP-SCI-V-205	42.99–43.00	0.00	0.00	75.84	24.16	silt loam
ICPP-SCI-V-213	37.50–37.51	0.00	1.09	80.91	17.98	silt loam
ICPP-SCI-V-213	37.58–37.59	0.00	1.12	79.93	18.96	silt loam
ICPP-SCI-V-213	37.65–37.69	0.00	0.82	80.09	19.10	silt loam
ICPP-SCI-V-213	37.69–37.74	0.00	1.36	78.79	19.83	silt loam
ICPP-SCI-V-213	37.79–37.80	0.00	0.00	79.40	20.59	silt loam
ICPP-SCI-V-213	37.80–37.82	0.00	0.11	79.51	20.35	silt loam
ICPP-SCI-V-213	37.91–38.00	0.00	0.03	80.78	19.19	silt loam
ICPP-SCI-V-213	38.00–38.02	0.00	0.00	80.24	19.77	silt loam
ICPP-SCI-V-213	38.02–38.03	0.00	0.00	77.54	22.46	silt loam
ICPP-SCI-V-213	38.03–38.04	0.00	0.00	79.56	20.44	silt loam
ICPP-SCI-V-213	38.04–38.06	0.00	0.00	79.76	20.22	silt loam
ICPP-SCI-V-213	38.06–38.08	0.00	0.00	79.78	20.23	silt loam
ICPP-SCI-V-213	38.08–38.09	0.00	0.00	79.13	20.92	silt loam
ICPP-SCI-V-213	38.09–38.11	0.00	0.04	80.26	19.67	silt loam
ICPP-SCI-V-213	55.79–56.00	0.00	17.37	70.80	11.84	silt loam
ICPP-SCI-V-213	56.00–56.03	0.00	19.56	70.88	9.60	silt loam
ICPP-SCI-V-213	56.03–56.05	0.00	22.48	68.96	8.58	silt loam
ICPP-SCI-V-213	56.05–56.08	0.00	7.94	80.25	11.83	silt
ICPP-SCI-V-213	56.08–56.14	0.00	9.11	74.88	16.04	silt loam
ICPP-SCI-V-214	39.26–39.30	0.00	7.26	79.09	13.65	silt loam
ICPP-SCI-V-214	39.30–39.32	0.00	9.47	77.42	13.10	silt loam
ICPP-SCI-V-214	39.32–39.35	0.00	6.03	80.49	13.46	silt loam
ICPP-SCI-V-214	39.35–39.38	0.00	8.11	78.74	13.15	silt loam
ICPP-SCI-V-214	39.39–39.40	0.00	14.41	74.18	11.45	silt loam
ICPP-SCI-V-214	39.40–39.50	0.00	10.34	76.43	13.18	silt loam
ICPP-SCI-V-214	39.55–39.59	0.00	9.55	76.92	13.54	silt loam
ICPP-SCI-V-214	39.59–39.61	0.00	6.84	79.32	13.85	silt loam
ICPP-SCI-V-214	39.61–39.63	0.00	10.58	77.01	12.39	silt loam
ICPP-SCI-V-214	43.75–43.79	0.00	18.48	66.26	15.28	silt loam
ICPP-SCI-V-214	43.79–43.81	0.00	25.24	61.99	12.79	silt loam
ICPP-SCI-V-214	43.81–43.82	0.00	15.42	70.82	13.77	silt loam
ICPP-SCI-V-214	43.82–43.85	0.00	8.43	72.86	18.66	silt loam

Table 4. Textural class percentages and nomenclature using the U.S. Department of Agriculture's soil classification system for 76 bulk and core samples—Continued

Borehole	Depth interval (m)	Gravel (> 2 mm) (%)	Sand (2-0.05 mm) (%)	Silt (0.05-0.002 mm) (%)	Clay (< 0.002 mm) (%)	Texture
ICPP-SCI-V-214	43.85–43.96	0.00	7.46	75.30	17.24	silt loam
ICPP-SCI-V-214	43.96–44.05	0.00	4.40	77.23	18.34	silt loam
ICPP-SCI-V-214	44.12–44.13	0.00	0.00	74.03	26.00	silt loam
ICPP-SCI-V-214	44.20–44.21	0.00	0.00	73.00	27.04	silty clay loam
ICPP-SCI-V-214	44.27–44.28	0.00	0.00	71.16	28.81	silty clay loam
ICPP-SCI-V-214	44.28–44.36	0.00	0.00	70.96	29.02	silty clay loam
ICPP-SCI-V-214	55.94–55.95	0.00	46.14	46.75	7.09	loam
ICPP-SCI-V-214	56.02–56.03	0.00	45.41	47.06	7.52	loam
ICPP-SCI-V-214	56.10–56.11	0.00	37.00	51.67	11.31	silt loam
ICPP-SCI-V-214	56.16–56.17	0.00	49.35	40.66	9.94	loam
ICPP-SCI-V-214	56.24–56.33	0.00	23.80	62.77	13.46	silt loam
ICPP-SCI-V-214	56.33–56.37	0.00	12.50	74.69	12.83	silt loam
ICPP-SCI-V-214	56.37–56.40	0.00	1.78	83.47	14.75	silt loam

Table 5. Specific surface areas for 10 core samples

[Specific surface area (s) is defined as the surface area (m^2) of sediment analyzed divided by the weight (g). Five points on the nitrogen adsorption isotherm were measured to calculate the surface areas according to Brunauer-Emmett-Teller (BET; 1938) theory.]

Borehole	Depth interval (m)	Specific surface area, s (m^2/g)
ICPP-SCI-V-189	36.59–36.69	49.87
ICPP-SCI-V-198	42.91–43.00	34.86
ICPP-SCI-V-204	48.41–48.49	38.13
ICPP-SCI-V-205	42.30–42.54	35.42
ICPP-SCI-V-213	37.91–38.00	23.65
ICPP-SCI-V-213	56.08–56.15	34.62
ICPP-SCI-V-214	39.40–39.50	24.96
ICPP-SCI-V-214	43.85–43.96	48.08
ICPP-SCI-V-214	43.96–44.05	50.36
ICPP-SCI-V-214	56.24–56.33	22.18

Table 6. Comparison of particle-size statistics between baked and non-baked sediment

[Baked and non-baked intervals were defined based on Munsell (1994) color and proximity to the tops of the interbeds (as noted in the lithologic log for each borehole). Average particle-size statistics (geometric mean and standard deviation) were calculated for the depth intervals identified as baked or non-baked, based on the listed number of samples used for particle-size measurement.]

Borehole	Top of interbed (m)	Depth interval analyzed (m)	Munsell color notation	Munsell color	Description	Average geometric mean particle size (mm)	Average geometric standard deviation	Number of samples
35-m interbed								
ICPP-SCI-V-189	36.59	36.59–37.04	7.5YR 6/6	reddish yellow	baked	0.0156	4.45	2
ICPP-SCI-V-198	37.80	42.84–43.29	2.5Y 7/4	pale yellow	non-baked	0.0038	2.95	8
ICPP-SCI-V-205	38.41	42.23–43.00	2.5Y 7/3	pale yellow	non-baked	0.0039	2.98	11
ICPP-SCI-V-213	37.50	37.50–38.11	7.5YR 6/6	reddish yellow	baked	0.0054	3.34	14
ICPP-SCI-V-214	39.63	39.26–44.36	10YR 7/3	very pale brown	non-baked	0.0085	3.84	19
45-m interbed								
ICPP-SCI-V-204	46.04	48.32–48.74	10YR 7/3 to 7/4	very pale brown	non-baked	0.0065	3.17	10
ICPP-SCI-V-215	45.24	45.53–45.95	7.5YR 6/6	reddish yellow	baked	0.0968	7.82	3
ICPP-SCI-V-215	45.24	46.10–47.49	7.5YR 6/4 to 6/6	light brown to reddish yellow	non-baked	0.0463	5.79	5
55-m interbed								
ICPP-SCI-V-213	54.27	55.79–56.14	10YR 6/4 to 7.5YR 6/4	light yellowish brown to light brown	non-baked	0.0131	4.03	5
ICPP-SCI-V-214	55.79	55.94–56.03	5YR 5/6 to 5/8	yellowish red	baked	0.0312	4.72	2
ICPP-SCI-V-214	55.79	56.10–56.40	7.5YR 6/4	light brown	non-baked	0.0170	4.92	5
ICPP-SCI-V-215	57.29	58.36–59.30	2.5YR 5/6 to 6/6	red to reddish yellow	baked	0.1200	3.69	3
ICPP-SCI-V-215	57.29	59.48–60.02	7.5YR 5/4 to 7.5YR 6/4	strong brown to light brown	non-baked	0.1053	5.68	3